High-Resolution Observations and Model Simulations of the Life Cycle of an Intense Mesoscale Snowband over the Northeastern United States

DAVID R. NOVAK

Scientific Services Division, NOAA/National Weather Service/Eastern Region, Bohemia, and School of Marine and Atmospheric Sciences, Stony Brook University, Stony Brook, New York

BRIAN A. COLLE

School of Marine and Atmospheric Sciences, Stony Brook University, Stony Brook, New York

SANDRA E. YUTER

Department of Marine, Earth, and Atmospheric Sciences, North Carolina State University at Raleigh, Raleigh, North Carolina

(Manuscript received 19 April 2007, in final form 3 August 2007)

ABSTRACT

This paper investigates the structural and dynamical evolution of an intense mesoscale snowband occurring 25–26 December 2002 over the northeastern United States. Dual-Doppler, wind profiler, aircraft, and water vapor observations in concert with the fifth-generation Pennsylvania State University–NCAR Mesoscale Model run at 4-km grid spacing are used to highlight evolutionary aspects of a snowband unresolved by previous studies. The high-resolution observations and model simulations show that band formation was coincident with a sharpening of a midlevel trough and associated increase in frontogenesis in an environment of conditional and inertial instability. Band maturity was marked by increasing conditional stability and a threefold increase in frontogenetical forcing. Band dissipation occurred as the midlevel trough and associated frontogenetical forcing weakened, while the conditional stability continued to increase. The effect of changing ascent is shown to dominate over changing moisture in explaining band dissipation in this case. Unconventional aspects of band structure and dynamics revealed by the high-resolution data are discussed, including the location of the band relative to the frontogenesis maximum, increasing stability during the band-formation process, and the presence of inertial instability. The model realistically predicted the band evolution; however, maximum precipitation was underforecast within the banded region by ~30% at 4-km grid spacing, and the axis of heaviest precipitation was displaced ~50 km to the southeast of the observed location. Higher horizontal model resolution is shown to contribute toward improved QPF in this case; however, it appears more dramatic improvement may be gained by better simulating the frontogenesis, stability, and moisture evolution.

1. Introduction

Understanding the dynamics of mesoscale precipitation systems and their predictability is a key research objective for improving cool-season quantitative precipitation forecasts (QPF) (Ralph et al. 2005). Meso-β-scale precipitation bands resulting from frontal circulations have proven difficult to forecast (Weismueller and Zubrick 1998; Nicosia and Grumm 1999, hereinafter NG99). Such bands have dramatic effects on the intensity, timing, and subsequent accumulation of precipitation. These effects are especially evident during the cool season, when the occurrence of snowbands often results in intense snowfall and extreme snowfall gradients (Kocin and Uccellini 2004, 177–186). Therefore, improving understanding of the structural and dynamical evolution of cool-season mesoscale bands can advance cool-season QPF skill.

Cool-season banded precipitation occurs in a variety of types (e.g., Houze et al. 1976; Browning 1990; Hobbs et al. 1996). In a cool-season climatology of banded

Corresponding author address: David R. Novak, NOAA/NWS/Eastern Region Headquarters, Suite 202, 630 Johnson Ave., Bohemia, NY 11716.
E-mail: david.novak@noaa.gov

DOI: 10.1175/2007MWR2233.1

events in the northeastern United States, Novak et al. (2004) found that the most common band type was the single-banded structure, often observed in the comma-head portion of developing cyclones. The single-banded structure was defined as a linear reflectivity feature 20–100 km in width and greater than 250 km in length, which maintains a minimum intensity of 30 dBZ along a majority of its length for at least 2 h. This structure may locally exhibit multibanded features that merge into a single dominant band axis (Novak et al. 2004). The single-banded structure has also been observed in Atlantic Canada (Reuter and Yau 1990; Stewart 1991) and the central United States (Martin 1998a,b; Moore et al. 2005).

Conditional symmetric instability (CSI; Bennetts and Hoskins 1979) has often been cited as a contributing factor in banded precipitation (Schultz and Schumacher 1999). However, theoretical work by Emanuel (1985), Thorpe and Emanuel (1985), and Xu (1989, 1992) has established that symmetric instability need not be present for single-band formation to occur. Rather, intense single bands can form through a coupled relationship between frontogenesis and moist symmetric stability, whereby the ascending branch of a frontal circulation is dramatically narrowed and enhanced when weak moist symmetric stability is present on the warm side of a frontal boundary. Consistent with these theoretical results, observations of band formation in the comma-head portion of eastern U.S. cyclones (e.g., Sanders and Bosart 1985; Martin 1998a,b; NG99; Novak et al. 2004; Moore et al. 2005; Grim et al. 2007) show band formation to be associated with deformation and associated frontogenetical forcing in the presence of weak moist symmetric stability.

Although a basic understanding of the fundamental processes responsible for band formation within the comma-head portion of cyclones has been established, questions remain concerning how changes in forcing, stability, and moisture relate to band life cycle. For example, band dissipation has been hypothesized to be a consequence of increasing symmetric stability (NG99) and weakening forcing (Novak et al. 2004); however, the limited temporal and spatial resolution of past studies has precluded testing these hypotheses. There is also limited knowledge of the 3D band structure and its evolution. For instance, previous studies have stated that bands form on the warm side of a midlevel frontogenesis maximum (Sanders and Bosart 1985; Jurewicz and Evans 2004; Moore et al. 2005, their Fig. 15a). These statements are supported by idealized frontal studies employing the Sawyer–Eliassen equation (Sawyer 1956; Eliassen 1962), which show the strongest ascent 50–200 km to the warm side of the frontogenesis maximum (e.g., Emanuel 1985; Thorpe and Emanuel 1985; Xu 1992). However, these studies have used idealized frontogenetical forcing. Additionally, mesoscale processes such as hydrometeor advection may shift the precipitation band relative to the frontogenesis maximum. High-resolution observations could improve our understanding of the structural and dynamical evolution of cool-season mesoscale bands.

The advent of high-resolution modeling provides an opportunity to explore the structural and dynamical evolution of a mesoscale band on scales not readily observed. High-resolution modeling of observed mesoscale banding events in the comma-head portion of cyclones has been rare (e.g., Baxter and Graves 2006; Han et al. 2007). Past modeling studies exploring the evolution of frontogenesis (Moore et al. 2005; Han et al. 2007), stability reduction in the comma-head portion of cyclones (Cao and Cho 1995; NG99; Clark et al. 2002), and moisture sources (Moore et al. 2005) have used horizontal grid spacing coarser than 25 km. At these coarse resolutions the mesoscale forcing may not be fully resolved, and the ability of a model to simulate the release of moist symmetric instability is compromised (Persson and Warner 1993; Schultz and Schumacher 1999). Also, these resolutions are not sufficient to resolve sharp gradients in moisture observed within the warm-frontal region of cyclones (e.g., Grim et al. 2007).

This study uses dual-Doppler, wind profiler, commercial aircraft, and integrated precipitable water vapor observations in concert with model simulations at 4-km grid spacing to investigate the structural and dynamical evolution of an intense mesoscale snowband. These datasets will be used to highlight aspects of band structure and dynamics unresolved by previous studies, including the development of a sharp midlevel trough during band formation, an unconventional location of the band relative to the frontogenesis maximum, and the presence of increasing stability during the band-formation process. The availability of high-resolution observations and model simulations further allows the diagnosis of model error in this case.

The mesoscale snowband studied in this paper occurred from 25 to 26 December 2002 over central and eastern New York. Storm total snowfall accumulations exceeded 90 cm in some locations, with much of this snow falling during a 6-h period associated with the formation of an intense mesoscale snowband. Operational forecast aspects of this case are reviewed in Novak et al. (2006) and Stuart and Grumm (2006).

Investigation of the 25–26 December 2002 banded event will be used to answer the following specific questions:

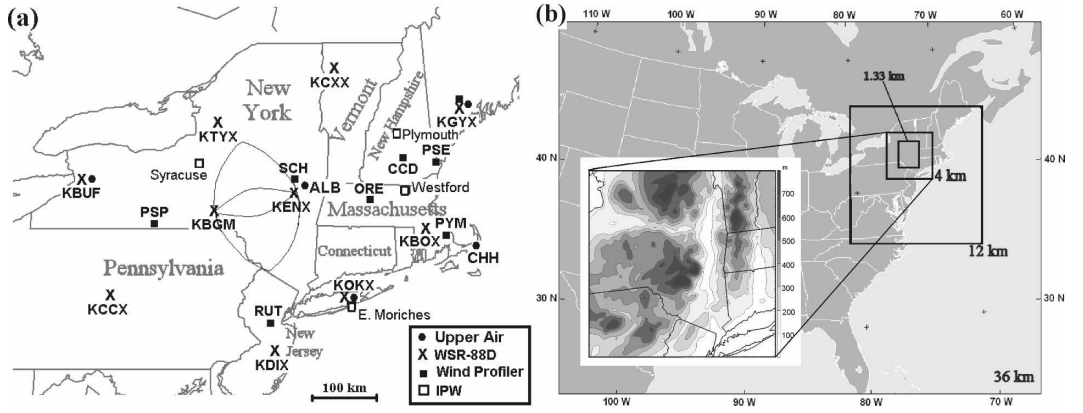

FIG. 1. (a) Station identifiers and locations of upper-air sounding (dots), WSR-88D ("x"), wind profiler (filled squares), and integrated precipitable water vapor (open squares) observation sites used in the study. The dual-Doppler coverage area is outlined between KBGM and KENX. (b) The 36-km model simulation domain, with inner boxes outlining locations of the 12-, 4-, and 1.33-km nested domains, respectively. Insert shows the terrain (m) of the 4-km domain.

- How does the frontogenesis, moist symmetric stability, and moisture change during band life cycle in this case?
- What was the observed structural evolution of the band during its life cycle?
- Can a high-resolution model simulate the structural and dynamical evolution of the band in this case?
- What were the model errors associated with band prediction in this case?

Section 2 describes the observational datasets and modeling configuration used in the study. Section 3 presents a multiscale overview of the case, and section 4 focuses specifically on the band life cycle, with particular emphasis placed on the evolution of frontogenesis and stability. Section 5 explores changes in moisture availability during the banded event, and a summary and discussion are provided in section 6.

2. Datasets and methodology

a. Observational datasets

The conventional surface and upper-air observation network was supplemented with Doppler radar, wind profiler, commercial aircraft, and ground-based integrated precipitable water vapor (IPW) observations (Fig. 1a) to better depict the structural and dynamical evolution of the 25–26 December 2002 banded event, and verify model forecasts.

Reflectivity and radial velocity data were obtained from Weather Surveillance Radar-1988 Doppler (WSR-88D) radar sites in the northeastern United States. These radars (Fig. 1a) provided nine elevation slices with a beamwidth of 1° and bin length of 1 km (0.25 km for velocity data; Klazura and Imy 1993). The WSR-88D velocity–azimuth display wind profile (VWP) product (Klazura and Imy 1993, their Fig. 12) was used to determine wind profiles at the WSR-88D radar sites.

The relatively close proximity of the Binghamton, New York, (KBGM) and Albany, New York, (KENX) radar sites to each other (165 km) allowed for dual-Doppler synthesis, following the methodology of Yuter and Houze (1995). The WSR-88D polar radar data from KBGM and KENX were interpolated to a common Cartesian grid at 2-km horizontal and 1-km vertical resolution. The wind field was computed up to a height of 10 km MSL within dual-Doppler lobes over eastern New York (Fig. 1a) using Custom Editing and Display of Reduced Information in the Cartesian Space (CEDRIC; Mohr et al. 1986) software. A two-step Leise filter (Leise 1982) was applied to eliminate wavelengths less than 8 km. Unfortunately, the relatively coarse vertical resolution of the WSR-88D scans prohibited acquisition of reliable vertical velocity magnitudes.

Additional wind observations were obtained from commercial aircraft (Moninger et al. 2003) and several 915-MHz boundary layer wind profilers (Fig. 1a) operating as part of the New England High-Resolution Temperature Program (Stensrud et al. 2006). Ground-based IPW retrievals (Gutman et al. 2004) from four stations near the banded event (Fig. 1a) were also available to aid verification of the model moisture fields.

Analyses from the Rapid Update Cycle (RUC; Benjamin et al. 2004) and National Centers for Environmental Prediction (NCEP) Eta Data Assimilation System (EDAS; Rogers et al. 2001) were compared with observations to determine the most representative

analyses. This investigation found that the EDAS analyses were superior to the RUC analyses for this case, with a better match of the wind profiler, aircraft, and radar-derived winds near the band. This behavior may be expected given the smaller grid spacing of the EDAS (12 km) relative to the RUC (20 km) and the more sophisticated analysis scheme used in the EDAS [three-dimensional variational data assimilation (3DVAR)] as compared with the RUC (optimum interpolation) at the time of this case (S. Benjamin 2006, personal communication). Therefore, EDAS analyses and Eta 3-h forecasts will be shown in this study, with both referred to as the analysis.

b. Model configurations

Model simulations of the 25–26 December 2002 banded event were run using the fifth-generation Pennsylvania State University–National Center for Atmospheric Research (NCAR) Mesoscale Model (MM5, version 3.4; Dudhia 1993) and Weather Research and Forecasting (WRF, version 2.0.3; Michalakes et al. 2001) model. The simulations were run using an outer 36-km domain covering the eastern two-thirds of the United States and adjacent coastal waters, and 12-, 4-, and 1.33-km nested (one way) domains centered on the banding location over eastern New York (Fig. 1b). Thirty-three sigma levels were used in the vertical, with maximum resolution in the boundary layer. The model top was set at 100 hPa. Model terrain was analyzed for the 36-, 12-, 4-, and 1.33-km grids from a 5′ and 30″ terrain dataset, respectively, using a Cressman analysis scheme, and filtered by a two-pass smoother–desmoother. Terrain from the 4-km model domain is shown in Fig. 1b. A 30″ land use dataset from NCAR was used to initialize 25 surface categories for all domains. The 4- and 1.33-km nests were run without convective parameterization.

The MM5 and WRF models were initialized with the 0000 UTC 25 December 2002 EDAS analysis, interpolated to the NCEP-221 grid (32-km horizontal resolution, 25-hPa vertical resolution). To explore whether mesoscale models are capable of predicting snowbands, the 0000 UTC 25 December 2002 Eta forecast (as opposed to a series of analyses) was used for boundary conditions. The boundary conditions were obtained by linearly interpolating the Eta forecast at 3-h intervals on the NCEP-104 grid (90-km horizontal resolution, 25-hPa vertical resolution). The U.S. Navy Optimum Thermal Interpolation System (OTIS) sea surface temperature analyses (~30-km horizontal resolution) were used to initialize the model surface temperatures over water.

The sensitivity of band formation and evolution to model physics schemes was investigated by varying the convective, boundary layer, and microphysics schemes in both the MM5 and WRF. The solutions clustered primarily by model type, with the WRF simulations providing a more accurate forecast of the surface cyclone central pressure and precipitation maximum than the MM5 simulations. However, the forecast banded event in the WRF simulations was composed of two short-lived (2-h duration) bands, which were not observed. Also, the bands and associated precipitation maxima in the WRF simulations were displaced ~200 km south of the observed maximum (Novak and Colle 2005). Thus the MM5 simulations were preferred. Differences of band characteristics between MM5 forecasts using different physics schemes were small, with storm total precipitation differences generally ranging less than 5 mm in the banding region; however, it was concluded that the Grell convective parameterization (Grell 1993), NCEP Medium-Range Forecast (MRF) boundary layer scheme (Hong and Pan 1996), and simple ice microphysics (Dudhia 1989; Hong et al. 2004) gave the most realistic simulation of band life cycle. Results from this simulation are discussed in the subsequent sections of this paper.

c. Calculations

The simplified 2D form of the Miller (1948) frontogenesis equation,

$$F_{2D} = \frac{1}{|\nabla\theta|}\left[-\frac{\partial\theta}{\partial x}\left(\frac{\partial u}{\partial x}\frac{\partial\theta}{\partial x} + \frac{\partial v}{\partial x}\frac{\partial\theta}{\partial y}\right) - \frac{\partial\theta}{\partial y}\left(\frac{\partial u}{\partial y}\frac{\partial\theta}{\partial x} + \frac{\partial v}{\partial y}\frac{\partial\theta}{\partial y}\right)\right], \quad (1)$$

is used to assess frontal forcing for ascent. The magnitude of (1) is identical to the magnitude of the across-isentropic component of the **Q**-vector Q_n when the geostrophic wind is substituted (Keyser et al. 1992; Martin 1999). Given the mesoscale nature of the problem in this work, the full wind will be used in calculating frontogenesis.

Moist symmetric stability is assessed through calculation of the saturation equivalent potential vorticity (EPV), defined as

$$\mathrm{EPV} = g\eta \cdot \nabla\theta_{es}, \quad (2)$$

where g is gravity, η is the three-dimensional absolute vorticity vector, and $\nabla\theta_{es}$ is the three-dimensional gradient of saturation equivalent potential temperature. Following Novak et al. (2004), the full wind will be used in calculating EPV since the full wind is likely to be

more representative than the geostrophic wind in evaluating moist symmetric stability in the sharply curved flow environments of bands in northeastern U.S. cyclones.

3. Case overview

a. Synoptic-scale evolution

Cyclone development during the 25–26 December 2002 banded event was similar to a Miller type-B cyclogenesis event (Miller 1946), which is characterized by coastal redevelopment of a surface cyclone as a 500-hPa trough approaches the eastern United States. At 1200 UTC 25 December 2002 (hereinafter, times will be abbreviated "time UTC/day"—1200/25 in this circumstance), a deep 500-hPa trough was present over the eastern United States, with a short wave evident in the satellite imagery over the southeastern United States (Fig. 2a). A 75 m s^{-1} jet at 300 hPa was found at the base of the 500-hPa trough, and a 50 m s^{-1} jet was found in the downstream confluent zone over southeastern Canada (Fig. 2a). This is a common jet configuration for major northeastern U.S. cyclogenesis events (Kocin and Uccellini 2004, 117–120). Surface cyclogenesis was occurring along the Virginia coast (Fig. 3a) in the diffluent exit region of the southern jet, southeast of the parent surface cyclone over eastern Ohio. The MM5 12-h forecast largely predicted these features, although the analyzed 500-hPa trough was ~10 m deeper than forecast (cf. Fig. 2a and Fig. 2b) and coastal surface development was underpredicted by 2 hPa (cf. Fig. 3a and Fig. 3b).

By 1800/25, rapid cyclogenesis had occurred along the New Jersey coast under the poleward exit region of the 300-hPa jet streak and just ahead of the 500-hPa short-wave trough (Figs. 2c and 3c). The surface cyclone had developed a warm occlusion frontal structure and deepened from 995 hPa at 1200/25 (Fig. 3a) to 979 hPa at 1800/25 (Fig. 3c). Common cyclogenesis features were evident in the observed and simulated cloud patterns at this time, including the emergence of a comma head over New York and Pennsylvania and dry slot near the southern New Jersey coast (Figs. 2c,d). Although the MM5 forecast exhibited a nearly identical position of the short-wave trough and attendant 300-hPa jet, the analyzed trough was ~30 m deeper and the jet ~5 m s^{-1} slower (cf. Fig. 2c and Fig. 2d). These errors translated into an ~7-hPa underprediction of the surface cyclone (cf. Fig. 3c and Fig. 3d).

By 0000/26, the surface cyclone had deepened to 973 hPa (Fig. 3e), but had become nearly vertically aligned with the 500-hPa cyclone (Fig. 2e), limiting further development. A well-defined comma head and dry slot were evident in satellite imagery at this time over New York and Connecticut, respectively (Fig. 2e). The MM5 forecast exhibited a similar cloud pattern (Fig. 2f); however, the MM5 underforecast the cyclone development, with a 60 m and 9-hPa underprediction of the 500-hPa and surface cyclone, respectively (Figs. 2f and 3f). Despite this cyclone intensity error, the MM5 predicted a realistic band evolution as described below.

b. Mesoscale evolution

The analyzed mesoscale evolution of the 25–26 December 2002 banded event featured the formation of a 700-hPa low over eastern Pennsylvania by 1800/25 (Fig. 4a), and the development of a sharp trough extending northeast from this low center into southern New Hampshire. This trough formed between 1500–1800/25 over New Jersey and southern New England, and rotated cyclonically to the northwest (not shown). The associated 700-hPa flow configuration at 1800/25 was marked by strong southerly flow approaching 25 m s^{-1} on the southeast side of this trough, with weak and variable flow on the northwest side of this trough (not shown). This flow convergence was occurring in the presence of a 5°C $(100\ km)^{-1}$ temperature gradient, resulting in a band of intense 700-hPa frontogenesis [values approaching 4°C $(100\ km^{-1})\ h^{-1}$] stretching from northeastern Pennsylvania into southern New Hampshire (Fig. 4a). Heavy snowfall was occurring near this 700-hPa frontogenesis maximum (Fig. 4a), while farther to the southeast near the coast the reflectivity was enhanced by a bright band associated with a melting layer. The MM5 forecast the heavy snowfall[1] near the developing 700-hPa low, although the forecast trough axis was ~50–100 km farther south than observed (cf. Fig. 4a and Fig. 4b). The corresponding frontogenesis maximum was comparable in magnitude to the analyzed maximum.

By 2100/25, an intense snowband had developed just west of the analyzed 700-hPa trough (Fig. 4c), with ~25 m s^{-1} southeast winds to the east of the trough and ~7 m s^{-1} north winds to the west of the trough (Fig. 5a). This flow convergence and deformation in the presence of a temperature gradient resulted in 700-hPa frontogenesis values exceeding 7°C $(100\ km^{-1})\ h^{-1}$ (Fig. 5a), with the snowband occurring just to the west of the 700-hPa frontogenesis maximum (Fig. 4c). The MM5

[1] Simulated reflectivities were calculated using empirical relations based on the model cloud and precipitation mixing ratios as in Koch et al. (2005). Because of the uncertainties in obtaining the simulated reflectivity, only qualitative comparisons are made between observed and modeled reflectivity structures.

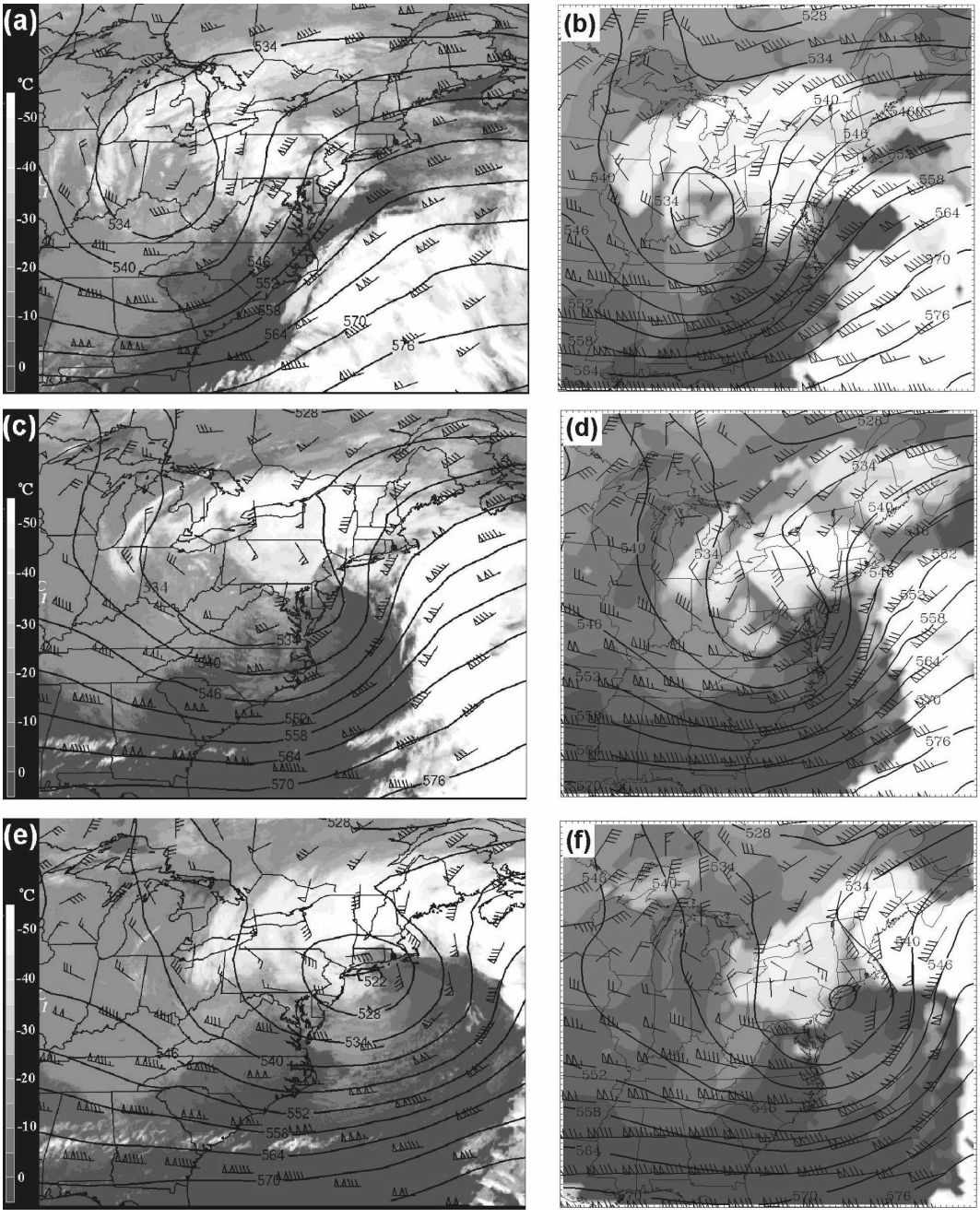

FIG. 2. Eta analysis of 500-hPa geopotential height (solid, contoured every 60 m), 300-hPa wind (full barb = 5 m s^{-1}, pennant = 25 m s^{-1}), and the infrared brightness temperature (°C, shaded) for (a) 1200 and (c) 1800 UTC 25 Dec 2002, and (e) 0000 UTC 26 Dec 2002. (b) As in (a), but for the 12-h MM5 forecast cloud-top temperature (shaded) valid at 1200 UTC 25 Dec 2002. (d) As in (b), but for the 18-h MM5 forecast valid at 1800 UTC 25 Dec 2002. (f) As in (b), but for the 24-h MM5 forecast valid at 0000 UTC 26 Dec 2002.

successfully forecast intense band development, but the band was ~50 km farther southeast than observed (cf. Fig. 4c and Fig. 4d). Similar to the analysis, the MM5 forecast trough served as a focus for frontogenesis (cf. Fig. 5a and Fig. 5b). However, the axis of maximum frontogenesis was forecast by the MM5 ~50 km farther southeast than analyzed, which is consistent with the position error of the forecast band.

By 0000/26, the analyzed 700-hPa frontogenesis maximum began to weaken as the 700-hPa trough became less defined, and the associated deformation weakened (Fig. 4e); however, a band of frontogenesis

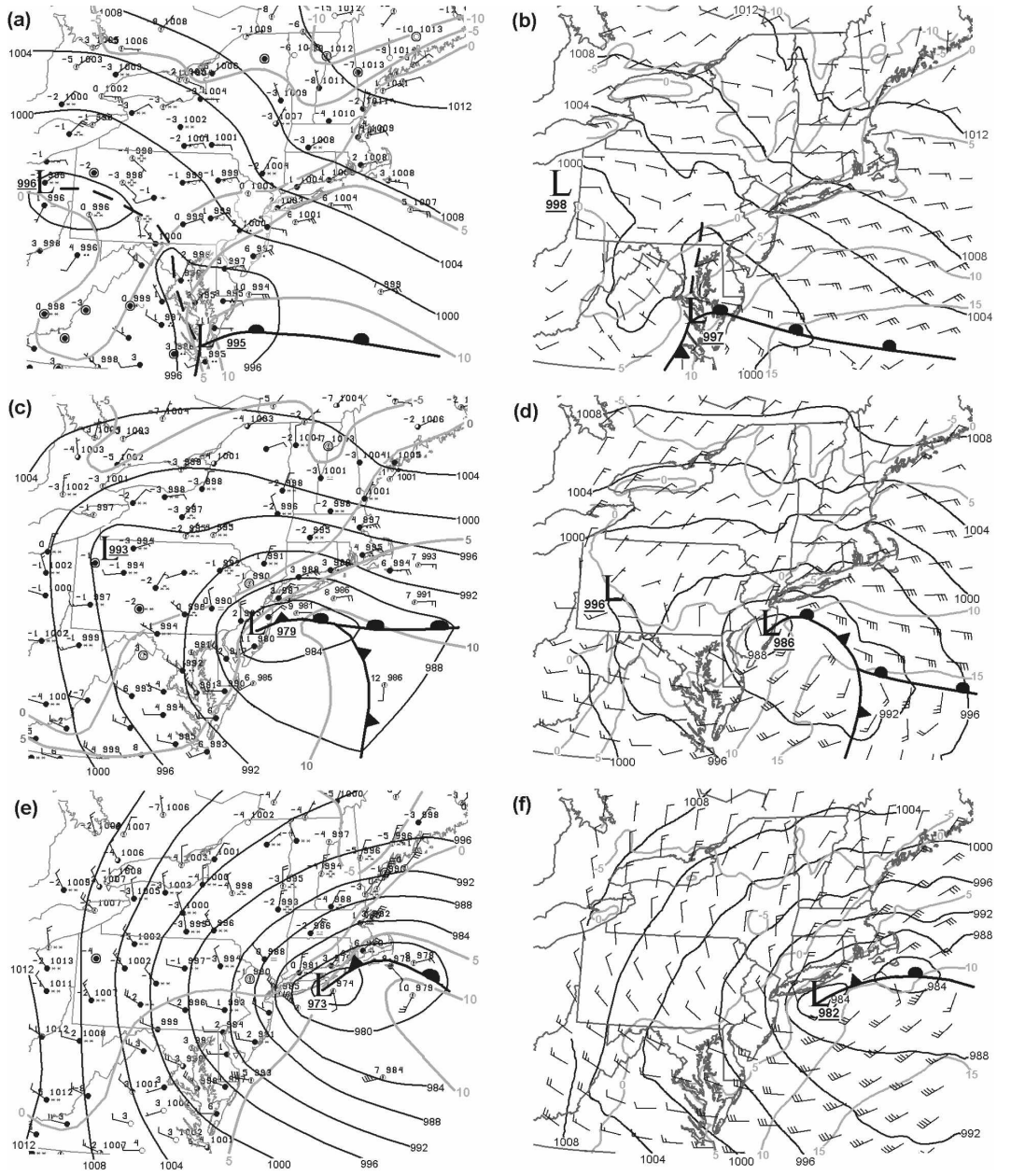

FIG. 3. Manual surface analysis with conventional surface station symbols, isobars (solid, contoured every 4 hPa), isotherms (gray, contoured every 5°C), and surface fronts valid at (a) 1200 and (c) 1800 UTC 25 Dec 2002, and (e) 0000 UTC 26 Dec 2002. (b) As in (a), but for the MM5 12-h forecast valid at 1200 UTC 25 Dec 2002. (d) As in (b), but for the 18-h MM5 forecast valid at 1800 UTC 25 Dec 2002. (f) As in (b), but for the 24-h MM5 forecast valid at 0000 UTC 26 Dec 2002.

still extended from eastern New York into Vermont and New Hampshire. The primary snowband remained just west of the analyzed 700-hPa frontogenesis maximum (Fig. 4e). Over the next 2.5 h, the frontogenesis continued to weaken and the snowband dissipated, with analyzed and forecast frontogenesis values of 4°C (100 km^{-1}) h^{-1} limited to the New York–Massachusetts border region (Figs. 4e,f). However, the MM5 forecast band dissipated at 0000/26, approximately 2.5 h earlier than observed.

c. QPF

The observed 24-h accumulated precipitation (liquid equivalent) ending 1200/26 exceeded 45 mm in a band

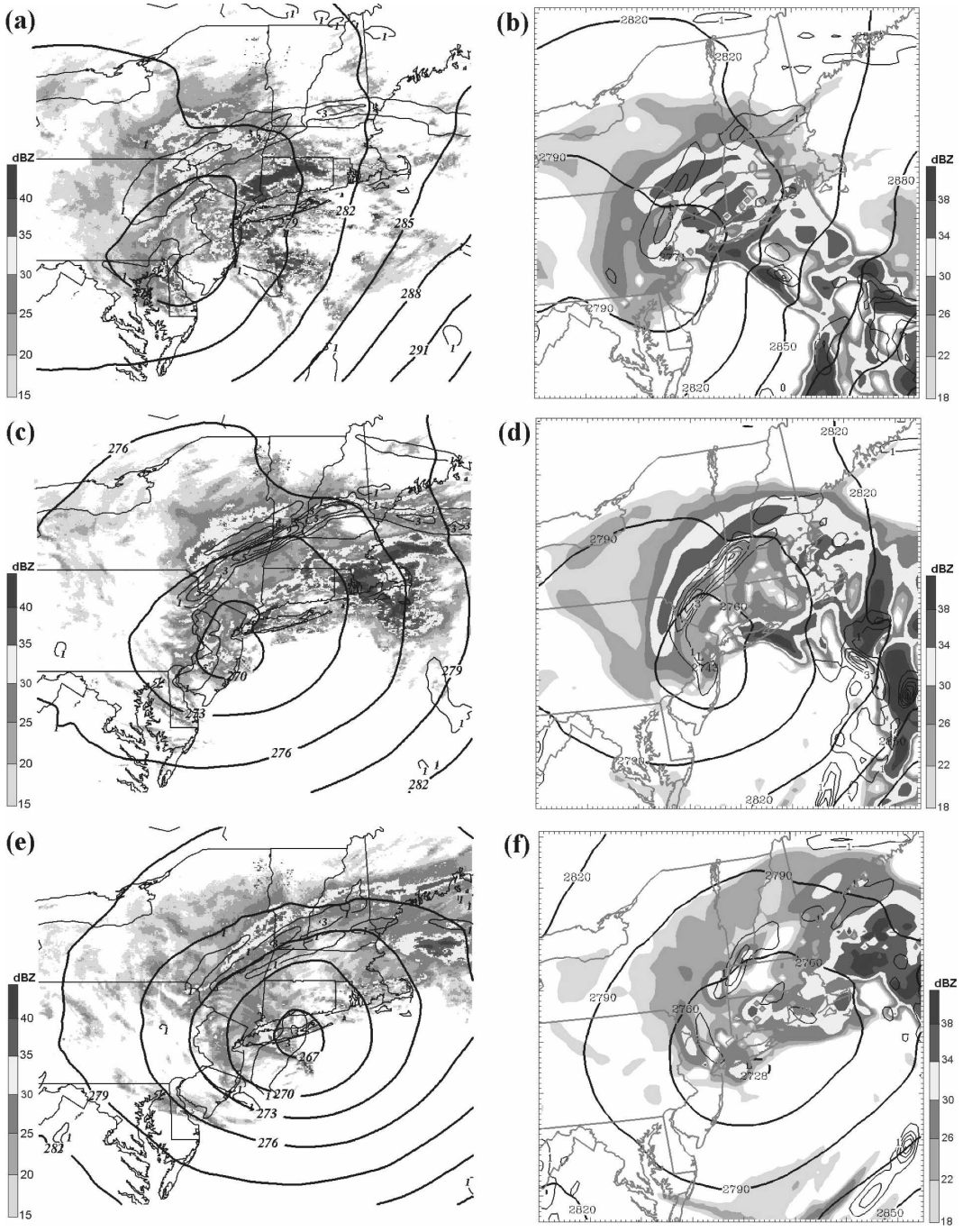

FIG. 4. WSR-88D radar mosaic (reflectivity shaded according to scale starting at 15 dBZ), with the Eta analysis 700-hPa geopotential height (thick solid, contoured every 30 m), and 700-hPa Miller 2D frontogenesis [thin solid, positive values contoured every 2°C (100 km)$^{-1}$ h^{-1} starting at 1°C (100 km)$^{-1}$ h^{-1}] overlaid, valid at (a) 1800 and (c) 2100 UTC 25 Dec 2002, and (e) 0000 UTC 26 Dec 2002. (b) The 12-km MM5 18-h forecast surface simulated reflectivity (shaded according to scale starting at 18 dBZ), 700-hPa geopotential height (thick gray, contoured every 30 m), and 700-hPa Miller 2D frontogenesis [thin solid, positive values contoured every 2°C (100 km)$^{-1}$ h^{-1} starting at 1°C (100 km)$^{-1}$ h^{-1}] valid at 1800 UTC 25 Dec 2002. (d) As in (b), but for the 12-km MM5 21-h forecast, valid at 2100 UTC 25 Dec 2002. (f) As in (b), but for the 12-km MM5 24-h forecast, valid at 0000 UTC 26 Dec 2002.

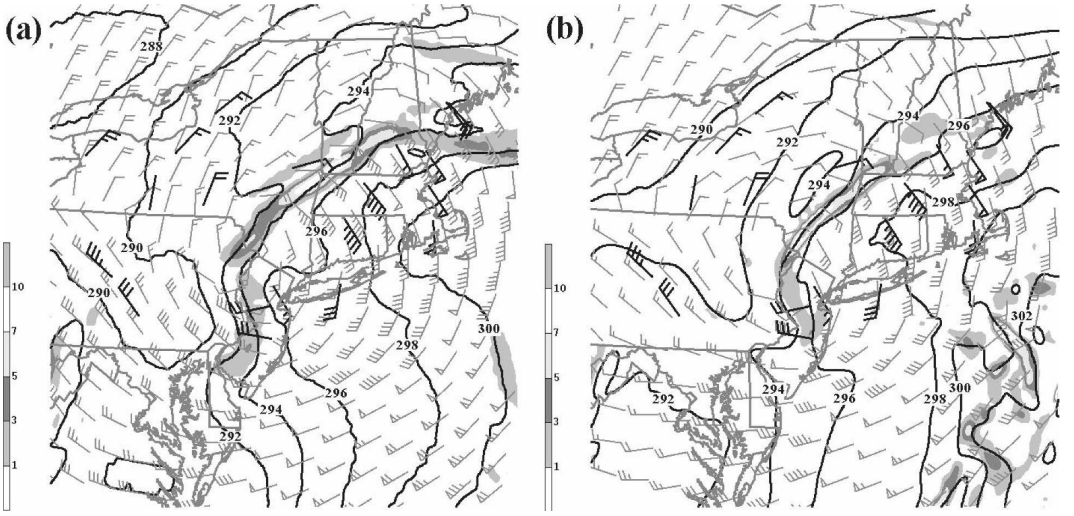

FIG. 5. (a) 2100 UTC 25 Dec 2002 Eta analysis of 700-hPa Miller 2D frontogenesis [shaded according to scale starting at 1°C (100 km)$^{-1}$ h^{-1}], 700-hPa potential temperature (solid, contoured every 2 K), and winds (gray barbs; full barb = 5 m s^{-1}, pennant = 25 m s^{-1}). In situ and remote sensing wind observations displayed as black barbs. (b) As in (a), but for the 12-km MM5 21-h forecast valid at 2100 UTC 25 Dec 2002.

stretching from northeastern Pennsylvania into eastern New York (Fig. 6a). An embedded maximum of 76 mm was located in eastern New York (Fig. 6a). The 12-km MM5 forecast accumulated precipitation band (Fig. 6b) was ~50 km to the east as compared with the observed location (Fig. 6a), which is consistent with the displaced forcing (e.g., Fig. 5). A second maximum of precipitation forecast in northern Connecticut was not observed (cf. Fig. 6a and Fig. 6b). The12-km MM5 forecast precipitation maximum within the band was 46 mm, which is ~40% less than observed. The corresponding 4- and 1.33-km MM5 precipitation fields exhibited a 53-mm (~30% underprediction) and 59-mm (~22% underprediction) maximum within the band (Figs. 6c and 6d, respectively), with greater spatial variance in precipitation likely from the improved representation of orographic effects (i.e., Fig. 1b). Thus, higher horizontal model resolution does result in improved QPF in this case, but it is not the sole answer.

Comparisons of bandwidth using simulated reflectivity fields averaged over the band life cycle showed a 15% reduction in bandwidth when reducing grid spacing from 12 to 4 km, but no further decrease when using 1.33-km grid spacing (not shown), suggesting the band was explicitly resolved at 4-km grid spacing. Therefore, the 4-km MM5 fields are used in the subsequent investigation of band life cycle.

4. Band life cycle

The band life cycle is subjectively divided into three stages—band formation, band maturity, and band dissipation. Timing differences of band dissipation between the model forecast and observations required comparing the 2300/25 model fields with the 0000/26 observed fields. Also, position differences in the maximum band intensity between the model forecast and observations necessitated different model and observed cross section locations.

a. Band formation

WSR-88D radar observations from the dual-Doppler synthesis at 1800/25 show a large region of enhanced precipitation in central New York (Fig. 7a). Animations over the subsequent 90 min showed enhanced reflectivity features moving toward the northwest and merging along a northeast–southwest axis, forming the primary band by 1929/25 (Fig. 8a). Examples of these enhanced reflectivity features are evident near the New Jersey–Pennsylvania border region (Fig. 7a), and in northeastern Pennsylvania (Fig. 8a), just southeast of the primary band. These band mergers and subsequent band formation occurred in a region of intense midlevel convergent flow associated with the midlevel trough (Fig. 4a). These convergent winds are evident in the dual-Doppler derived winds at 3 km MSL, where 25 m s^{-1} southeast winds slow to less than 5 m s^{-1} over a horizontal distance of 100 km (Fig. 7a), resulting in convergence of $\sim 2 \times 10^{-4}$ s^{-1}. This convergence is also evident in the wind profiler and aircraft observations across the region (Fig. 7a). By 1930/25 (Fig. 8a), the winds on the west side of the band turned to light northerly as the associated midlevel trough strengthened,

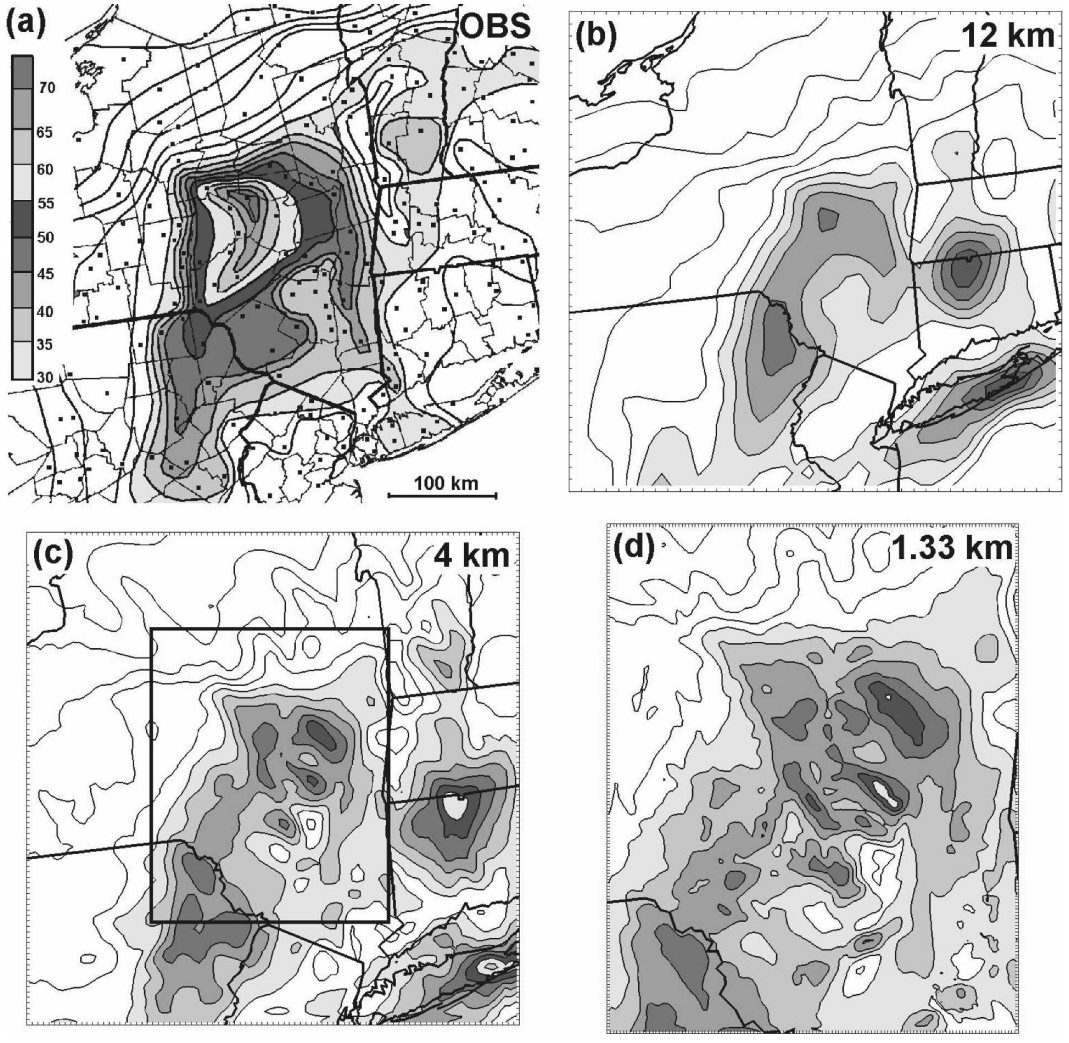

FIG. 6. (a) Observed liquid equivalent precipitation during the 24-h period ending 1200 UTC 26 Dec 2002 (contoured every 5 mm, shaded according to scale starting at 30 mm). Station observation locations used in the analysis are marked by black dots. Corresponding 12–36-h forecast accumulated precipitation shown for the (b) 12-, (c) 4-, and (d) 1.33-km MM5. Domain of (d) outlined by box in (c).

which effectively increased the deformation and maximum convergence to $\sim 2.4 \times 10^{-4}$ s^{-1}.

The 4-km MM5 forecast evolution of band formation is similar to the observations. At 1800/25, an east-northeast–west-southwest-oriented band was located in a region of speed convergence at 3 km MSL over eastern New York, while a second band was located farther southeast over western Connecticut (Fig. 7b). The first band weakened nearly in place over the next ~45 min, while the second band moved northwest into eastern New York, and became stretched along a northeast–southwest axis, forming the primary band by 1930/25 (Fig. 8b). The presence of light winds on the west side of the band at 1930/25 is similar to the dual-Doppler observations (cf. Fig. 8a and Fig. 8b).

At 1800/25, maximum frontogenesis values between 7° and 12°C (100 km)$^{-1}$ h^{-1} were located over southeastern New York, associated with speed convergence in the presence of a 2.3°C (100 km)$^{-1}$ temperature gradient (Fig. 7c). Ninety minutes later (Fig. 8c), the temperature gradient increased to ~2.7°C (100 km)$^{-1}$, and the convergence and deformation increased (related to the development of light winds on the west side of the trough). The combined effect was an increase in frontogenesis to values over 12°C (100 km)$^{-1}$ h^{-1} (Fig. 8c).

At 1800/25, a cross section of analyzed frontogenesis, ascent, and observed reflectivity through the band-formation region (Fig. 9a) shows that the frontogenesis maximum sloped from the surface (near the position of the warm occlusion) to 5 km MSL. This frontogenesis

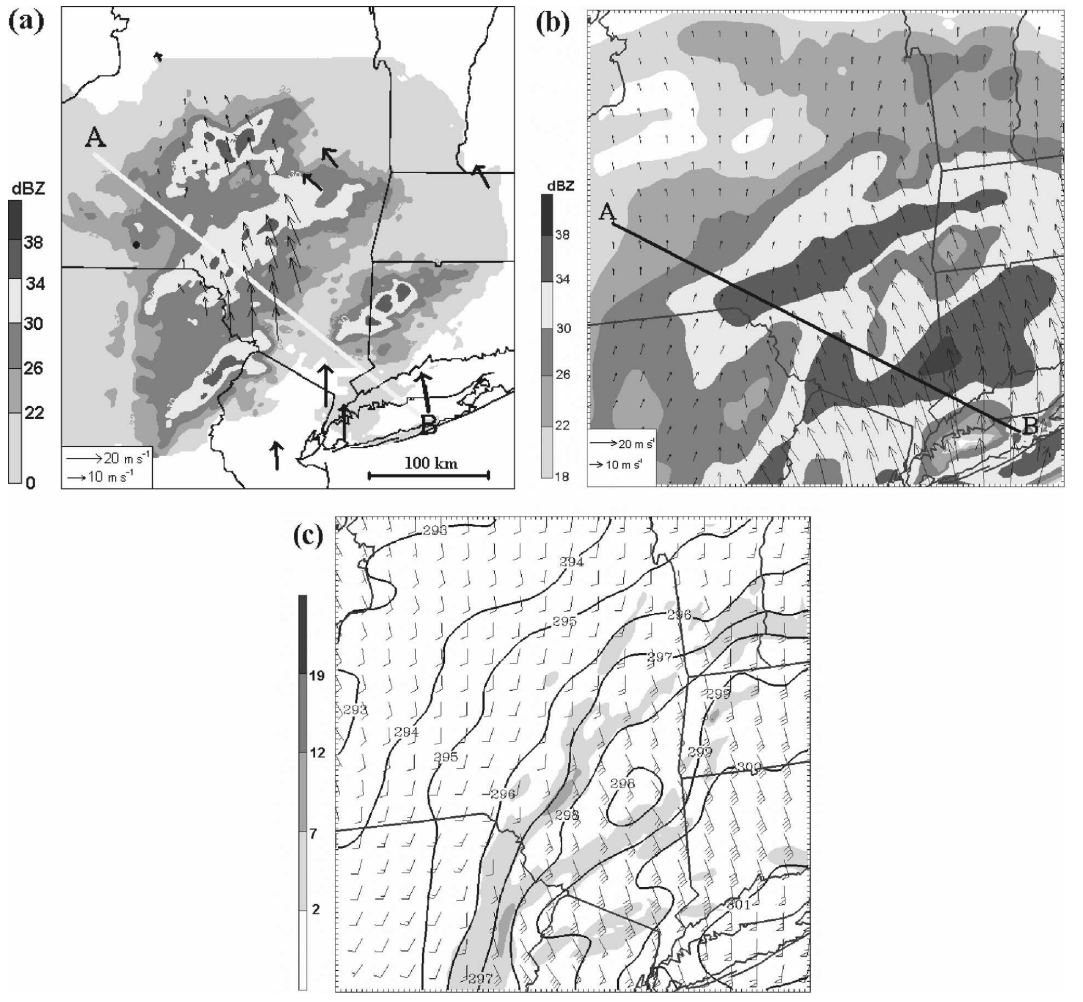

FIG. 7. (a) Dual-Doppler radar reflectivity (1-km-MSL altitude; shaded according to scale) and 3-km-MSL winds (arrows) valid at 1802 UTC 25 Dec 2002. In situ and remote sensing wind observations displayed as thick black arrows. (b) The 4-km MM5 18-h forecast simulated reflectivity (1-km-MSL altitude; shaded according to scale) and 3-km-MSL wind (arrows). (c) The 4-km MM5 18-h forecast Miller 2D frontogenesis [shaded according to scale starting at 2°C (100 km)$^{-1}$ h^{-1}], potential temperature (solid, contoured every 1 K), and wind (full barb = 5 m s^{-1}, pennant = 25 m s^{-1}) at 3 km MSL.

resulted in a relatively broad region of ascent, maximized at over 40 cm s^{-1} at a height of 5 km MSL (Fig. 9a). The resultant heavy snowfall occurred in a ~150–km-wide region, with the height of the observed 30 dBZ contour extending to nearly 5 km MSL (Fig. 9a). A region of negative EPV existed above the frontogenesis maximum in the 400–500-hPa layer (Fig. 9b), with the θ_{es} field indicating that much of this negative EPV region was associated with conditional instability (CI). A small portion of the CI region near 400 hPa at x = 300 km also exhibited negative absolute vorticity (calculated using the full wind), indicative of inertial instability (II). However, given the small area of II, CI was likely the dominant instability. Although this instability lies above the maximum frontogenesis, the vertical motion forced by frontogenesis extends well above the location of maximum frontogenesis (e.g., Sawyer 1956; Eliassen 1962; Thorpe and Emanuel 1985; Hakim and Keyser 2001). Thus, the observed heavy snowfall at 1800/25 was likely a result of the release of CI and II by frontogenetical forcing.

The corresponding 1800/25 4-km MM5 cross section (Figs. 9c,d) is similar to the analyzed 1800/25 cross section, with a sloping region of frontogenesis, associated ascent, and precipitation plume evident; however, the model cross section exhibits two distinct reflectivity bands near the surface at x = 120 km and x = 270 km (Fig. 9c). These reflectivity bands are associated with two separate ascent maxima, the strongest of which nears 80 cm s^{-1} (Fig. 9c). The ascent maxima and as-

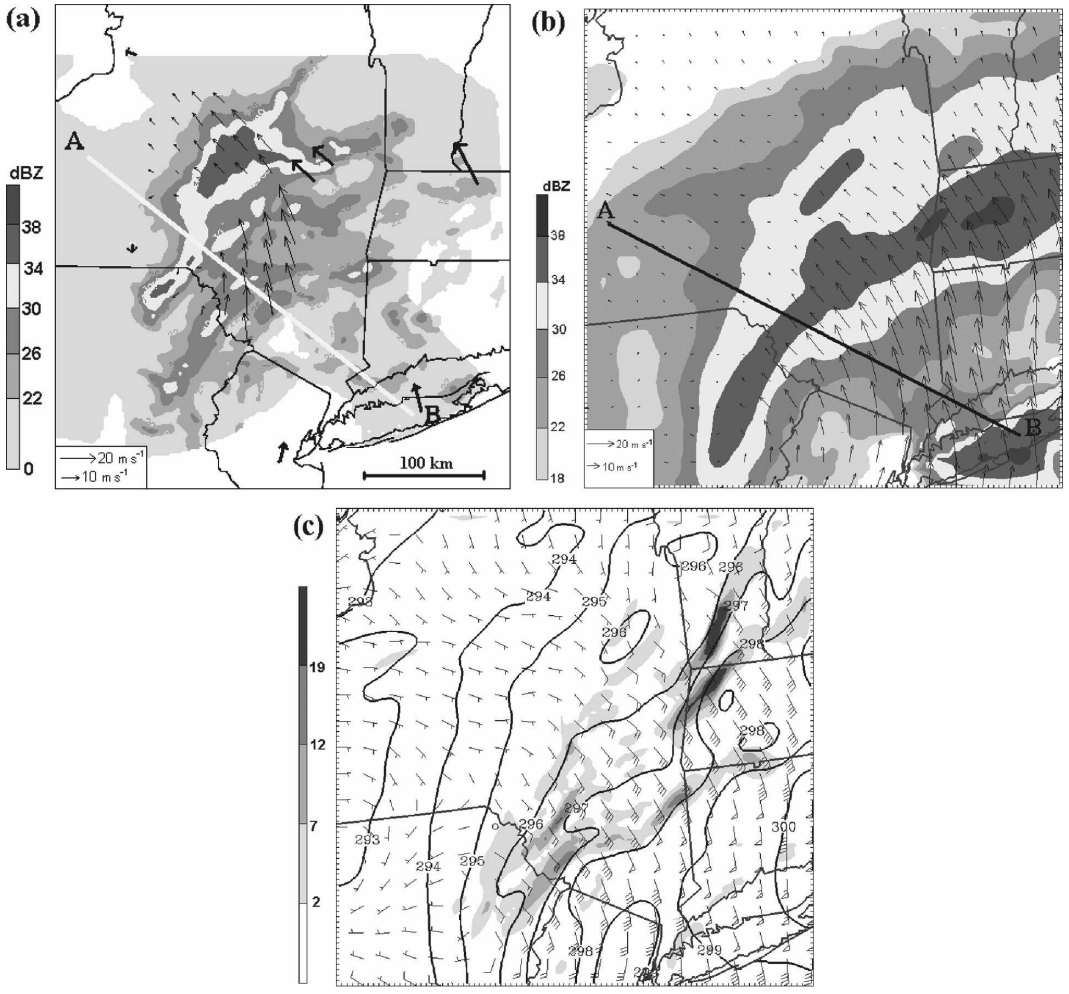

FIG. 8. (a) As in Fig. 7a, except valid at 1929 UTC 25 Dec 2002. (b), (c) As in Figs. 7b,c, but for the 19.5-h forecast valid at 1930 UTC 25 Dec 2002.

sociated bands are forced by two sloping frontogenesis maxima (Fig. 9c). These frontogenesis maxima correspond to two enhanced thermal gradients over southeastern New York at 3 km MSL (Fig. 7c). The corresponding MM5 cross section of the stability fields (Fig. 9d) indicates three regions of negative EPV in the 500–400-hPa layer. The first region ($x = 270$ km) is marked by both CI and II, whereas the second ($x = 180$ km) and third ($x = 100$ km) regions are marked by II. A large area of conditional neutrality exists between the first and second negative EPV minima in the region of strongest ascent. During the 1600–1800/25 period, elevated CI was diagnosed in this region (not shown). Thus, as shown in the Eta analysis, the modeled heavy snowfall at 1800/25 was likely a result of the release of CI and II by frontogenetical forcing.

By 1930/25 (Fig. 10a), the observed reflectivities evolved into a narrow and intense (>30 dBZ) band. The corresponding MM5 forecast shows that the double frontogenesis/ascent pattern and associated bands at 1800/25 had evolved into a single intense band, associated with a single frontogenesis/ascent maximum (Fig. 10b). The 4-km MM5 conditional stability at 1930/25 had generally increased during the past 90 min (cf. Fig. 9d and Fig. 10c); however, an ~30-km-wide region of negative EPV existed between 500 and 400 hPa on the equatorward edge of the ascent maximum. This negative EPV region coincides with a region of II.

b. Band maturity

The mature stage of the band life cycle occurred at 2100/25, when both the observed and modeled bands were near their peak intensity. At this time, the 3-km-MSL dual-Doppler winds exhibited a sharp cyclonic wind shift near the observed band, with strong southeast winds (17 m s^{-1}) on the east side of the band, and the emergence of 10 m s^{-1} north winds on the west side

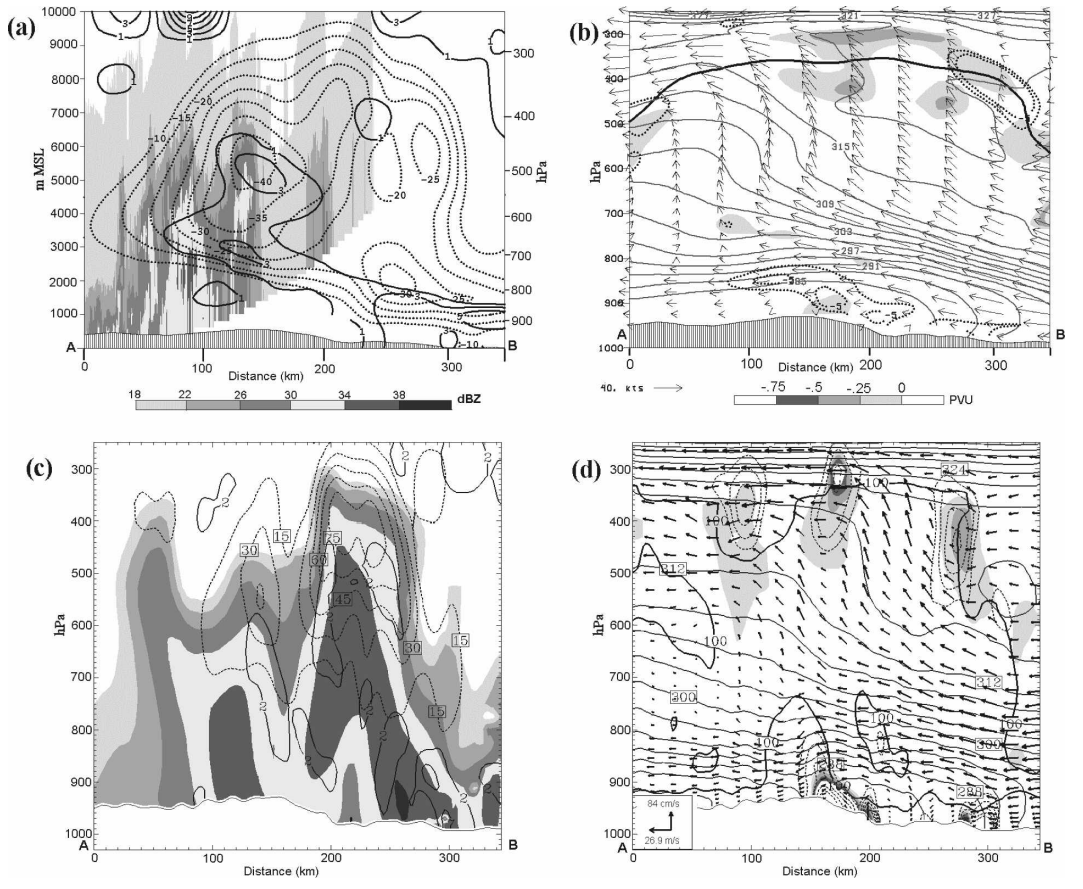

FIG. 9. (a) KBGM WSR-88D radar reflectivity cross section (orientation shown in Fig. 7a) valid at 1802 UTC 25 Dec 2002 with the 1800 UTC Eta analysis Miller 2D frontogenesis [solid, positive values contoured every 2°C (100 km)$^{-1}$ h^{-1}, starting at 1°C (100 km)$^{-1}$ h^{-1}], and ascent (dotted, contoured every 5 cm s^{-1} starting at 10 cm s^{-1}). (b) Cross section as in (a), with saturation equivalent potential vorticity (shaded where negative according to scale), saturation equivalent potential temperature (gray solid, contoured every 3 K), velocity in the plane of the cross section (arrows), absolute vorticity (dotted, contoured where negative every 5×10^{-5} s^{-1}), and the 100% contour of relative humidity w.r.t. ice (thick solid). (c) The 4-km MM5 18-h forecast cross section (orientation shown in Fig. 7b) showing simulated reflectivity [shaded according to scale, as in (a)], Miller 2D frontogenesis [black solid, positive values contoured every 4°C (100 km)$^{-1}$ h^{-1} starting at 2°C (100 km)$^{-1}$ h^{-1}], and ascent (dotted, contoured every 15 cm s^{-1} starting at 15 cm s^{-1}). (d) As in (b), but for the 4-km MM5 18-h forecast.

of the band (Fig. 11a). The position of this cyclonic wind shift, as well as the band, had moved eastward ~40 km during the past 90 min (cf. Fig. 8a and Fig. 11a).

The corresponding 4-km MM5 forecast also shows the establishment of a robust cyclonic wind shift near the simulated band (Fig. 11b). The magnitude of the temperature gradient had nearly tripled during the past 1.5 h, reaching a magnitude of ~8.3°C (100 km)$^{-1}$ within the region of maximum speed convergence just east of the trough axis (Fig. 11c). The large temperature gradient was created, in part, by the development of a local temperature minimum along a southwest–northeast axis nearly coincident with the band (Fig. 11c). Parcel trajectories and point temperature tendency calculations suggest that this local cooling was the result of the vertical advection of cooler air below the frontal inversion (in the 2–3-km-MSL layer) by the band updraft (not shown). The coincidence of this large temperature gradient with the zone of strong speed convergence resulted in frontogenesis values exceeding 19°C (100 km)$^{-1}$ h^{-1} (Fig. 11c).

A cross section of analyzed frontogenesis and ascent at 2100/25 (Fig. 12a) shows an intense frontogenesis maximum centered at 2.5 km MSL, with ascent nearing 30 cm s^{-1} above this level (Fig. 12a). The corresponding 4-km MM5 cross section at 2100/25 (Fig. 12c) is similar to the analysis cross section, with an intense frontogenesis maximum near 700 hPa and a narrow sloping updraft approaching 70 cm s^{-1} (Fig. 12c). Recall from section 1 that theory would predict the ascent maximum

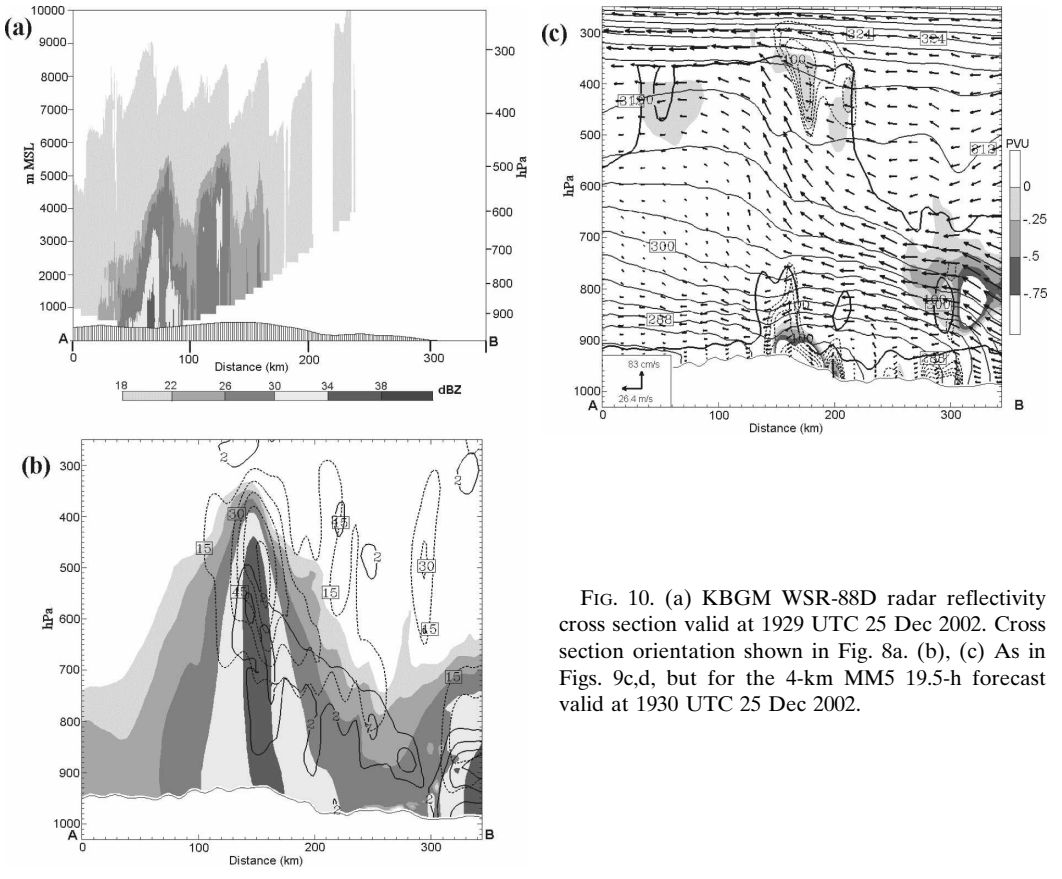

FIG. 10. (a) KBGM WSR-88D radar reflectivity cross section valid at 1929 UTC 25 Dec 2002. Cross section orientation shown in Fig. 8a. (b), (c) As in Figs. 9c,d, but for the 4-km MM5 19.5-h forecast valid at 1930 UTC 25 Dec 2002.

50–200 km to the warm side of the frontogenesis maximum. In the present case, both the observed and forecast ascent maximum is found nearly coincident with the frontogenesis maximum (Figs. 12a,c). This finding will be further discussed in section 6.

The 2100/25 cross section (Fig. 12a) also shows that the observed reflectivity core sloped downward to the west, such that the band core was ~10 km farther west at the surface than at 3 km MSL (Fig. 12a). Similar to these radar observations, the MM5 forecast band also exhibited a tilt, such that the band core was ~25 km farther west at the surface than at 3 km MSL (Fig. 12c). Explicit calculation of hydrometeor trajectories from the model forecast during the 1900–2100/25 period show that this displacement was due to horizontal advection of snow (Fig. 12c), with the band updraft slowing the hydrometeors' fall and prolonging the time the hydrometeors were subject to horizontal advection in the 600–500-hPa layer. Given the observed easterly component of the 3-km-MSL winds in the band region (e.g., Fig. 11a), hydrometeor advection is the most probable explanation for the observed band tilt. Model hydrometeor (snow) mixing ratios increased toward the surface, ranging from 0.3 g kg^{-1} at 450 hPa to a near-surface maximum of ~1.8 g kg^{-1} (not shown), qualitatively similar to the vertical structure of the observed radar reflectivity pattern (Fig. 12a).

The analyzed stability at 2100/25 indicates a large region of negative EPV on the warm side of the frontogenesis maximum in the 500–350-hPa layer (Fig. 12b). The elevated CI in the far southeast location (x = 300 km) transitions to a region of combined CSI and II in the central portion of the cross section (x = 200 km), and weak moist symmetric stability in the northwestern part of the cross section (x = 100 km). This distribution of stability is consistent with idealized schematics of stability regimes within a banded frontal zone (e.g., Schultz and Schumacher 1999; Moore et al. 2005). In contrast to the presence of CI and CSI at 2100/25 in the analysis, the MM5 forecast stability fields indicated conditional *stability* above the frontogenesis maximum at this time (cf. Fig. 12b and Fig. 12d). Although the juxtaposition of dry air over the saturated lower levels supported CI in the 600–700-hPa layer southeast of the banded region (Fig. 12d), the weak ascent (and even weak descent) in this region precluded the instability from being released in the MM5 forecast. Despite the conditional stability in the banded region at this time, a

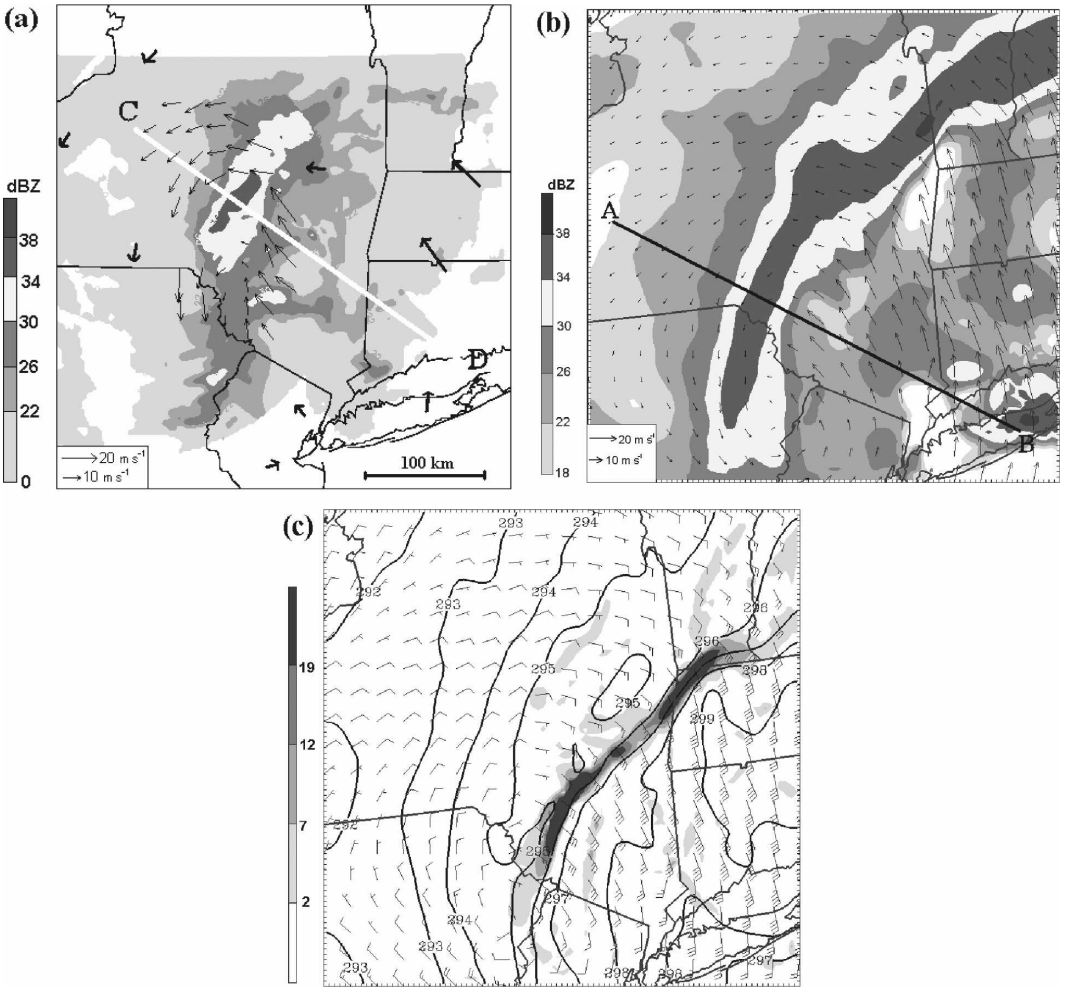

FIG. 11. (a) As in Fig. 7a, except valid at 2101 UTC 25 Dec 2002. (b), (c) As in Figs. 7b,c, but for the 4-km MM5 21-h forecast valid at 2100 UTC 25 Dec 2002.

relatively small area of negative EPV was found on the equatorward periphery of the sloping ascent maximum associated with II (Fig. 12d).

The presence of II in banded frontal zones has been shown in previous idealized and observational studies (e.g., Holt and Thorpe 1991; Persson and Warner 1995; Thorpe and Clough 1991; Jurewicz and Evans 2004; Schultz and Knox 2007). Holt and Thorpe (1991) proposed that upright convection can create II within frontal regions via the vertical advection of low momentum air. The ensuing slantwise flow response was termed "delta-M adjustment" (see also Morcrette and Browning 2006). In the present case, CI (representing the potential for upright convection) was present during band formation (e.g., Figs. 9b,c); however, during band maturity CI is absent in the MM5 forecast while II is present (Fig. 12d). Examination of the model fields shows that the forecast II at 450 hPa was within a 30–40-km-wide geopotential height ridge (~3-m amplitude), which was directly above a maximum in the 700–500-hPa layer-averaged condensational heating (associated with the snowband; Fig. 13). The positive height perturbations and associated anticyclonic flow are consistent with a diabatically generated ridge associated with diabatic heating by the band itself. Similar correspondence between condensational heating, height perturbations, and II were found at the time of band formation and dissipation (not shown). Given the presence of the II in the absence of upright convection, it seems likely that the diagnosed presence of II in the model forecast during band life cycle in this case is a diabatic signature of the band itself.

c. Band dissipation

At 0000/26, the weakening snowband was found near the New York–Massachusetts border, with the cy-

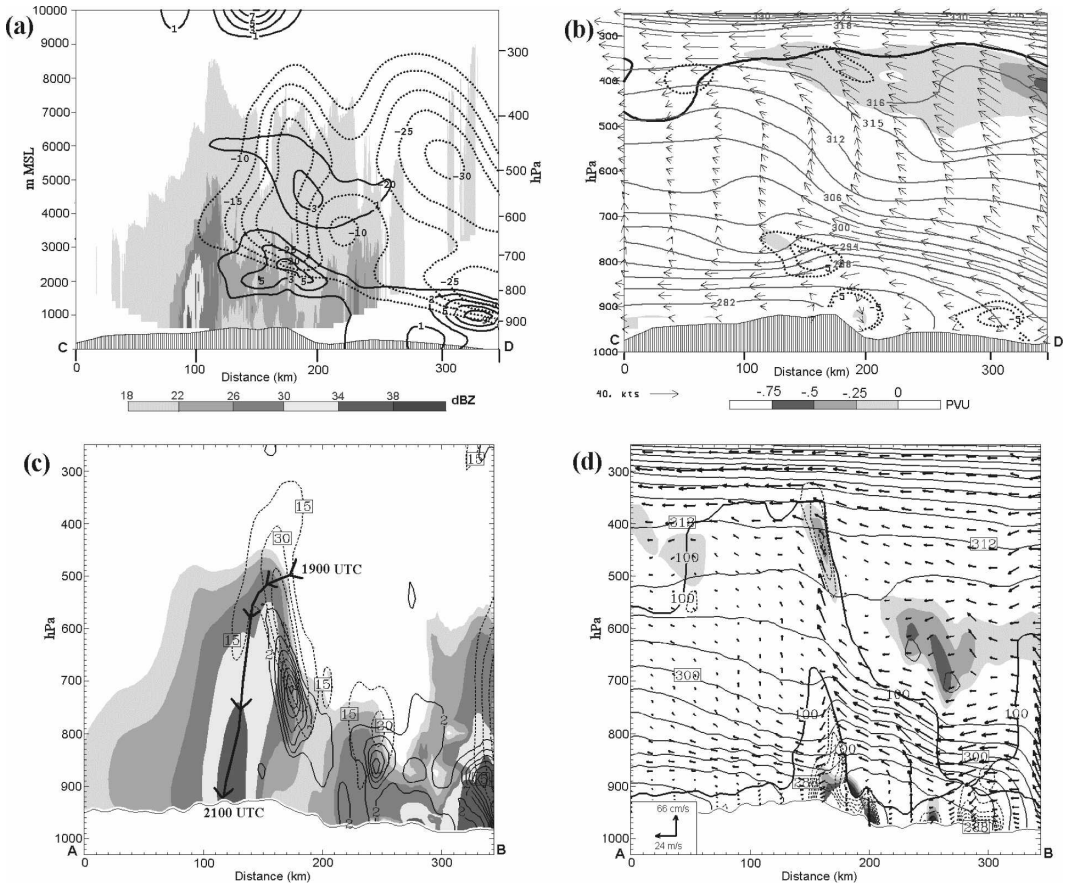

FIG. 12. (a) KENX WSR-88D radar reflectivity cross section (orientation shown in Fig. 11a) valid at 2101 UTC 25 Dec 2002 with the 2100 UTC Eta analysis Miller 2D frontogenesis [solid, positive values contoured every 2°C (100 km)$^{-1}$ h^{-1}, starting at 1°C (100 km)$^{-1}$ h^{-1}], and ascent (dotted, contoured every 5 cm s^{-1} starting at 10 cm s^{-1}). (b) Cross section as in (a), with saturation equivalent potential vorticity (shaded where negative according to scale), saturation equivalent potential temperature (gray solid, contoured every 3 K, except the 316-K potential temperature contour added for clarity), velocity in the plane of the cross section (arrows), absolute vorticity (dotted, contoured where negative every 5×10^{-5} s^{-1}), and the 100% contour of relative humidity w.r.t. ice (thick solid). (c) The 4-km MM5 21-h forecast cross section (orientation shown in Fig. 11b) showing simulated reflectivity [shaded according to scale, as in (a)], Miller 2D frontogenesis [black solid, positive values contoured every 4°C (100 km)$^{-1}$ h^{-1}, starting at 2.0°C (100 km)$^{-1}$ h^{-1}], ascent (dotted, contoured every 15 cm s^{-1} starting at 15 cm s^{-1}), and the 1900–2100 UTC 25 Dec 2002 hydrometer trajectory in the plane of the cross section (bold, arrows drawn every 0.5 h). (d) As in (b), but for the 4-km MM5 18-h forecast along section A–B (orientation shown in Fig. 11b).

clone's dry slot evident in eastern Connecticut and Massachusetts (Fig. 14a; see also Fig. 2e). Although the cyclonic wind shift had moved to the east of the dual-Doppler coverage area, wind observations from the Schenectady, New York (SCH), and Orange, Massachusetts (ORE), profilers (Fig. 1a) showed that the 3-km-MSL wind shift was aligned from southern New Hampshire through western Massachusetts (Fig. 14a). Southeast winds on the east side of this trough (15 m s^{-1} at ORE) were considerably weaker than during band formation or maturity (cf. Fig. 11a and Fig. 14a), resulting in reduced convergence, deformation, and associated frontogenesis relative to earlier times.

The MM5 forecast valid at 2300/25 shows the cyclonic wind shift had moved east ~50 km during the past 2 h (cf. Fig. 11b and Fig. 14b). Southeast winds on the east side of this trough were ~5 m s^{-1} less than observed (cf. Fig. 14a and Fig. 14b), and ~5 m s^{-1} less than during band maturity (cf. Fig. 11b and Fig. 14b). Localized maxima of convergence and deformation were found in western Massachusetts and southern New York, resulting in two frontogenesis maxima (Fig. 14c); however, the frontogenesis maxima were considerably weaker than at the time of band maturity (cf. Fig. 11c and Fig. 14c)

Cross sections through the observed and forecast

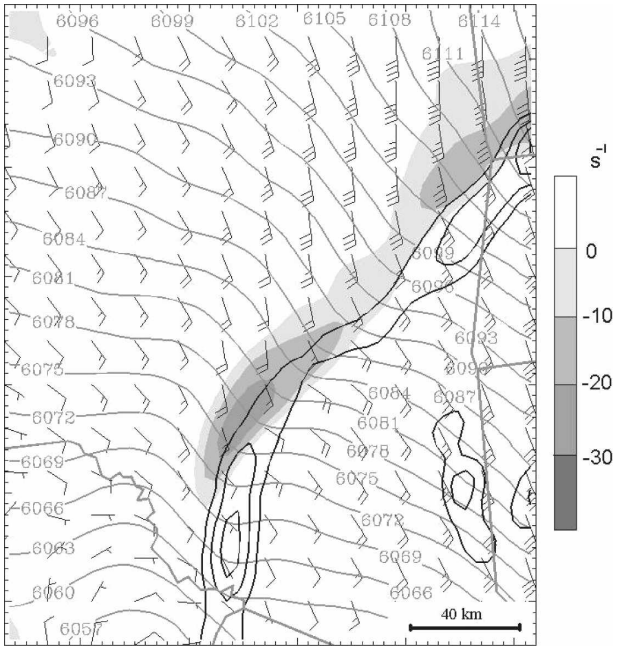

FIG. 13. The 4-km MM5 21-h forecast 450-hPa absolute vorticity (shaded where negative according to scale every 10×10^{-5} s^{-1}), geopotential height (gray solid, contoured every 3 m), winds (full barb = 5 m s^{-1}), and 700–500-hPa layer-averaged condensational heating rate (thin solid, contoured every 1°C h^{-1}, starting at 0°C h^{-1}).

band show that the frontogenesis and ascent had weakened from the time of band maturity (cf. Fig. 15a and Fig. 12a, and Fig. 15c and Fig. 12c). The analyzed stability had increased from the time of band maturity, with only a small region of CI found above the band in the 600–500-hPa layer (cf. Fig. 12b and Fig. 15b). CI was absent in the model stability fields in the banded region (Fig. 15d); however, once again a small area of negative EPV was found on the equatorward periphery of the sloping ascent maximum (Fig. 15d), associated with II.

d. Model time series

A time series of frontogenesis, ascent, and conditional stability during the life cycle of the simulated band was constructed to better understand its evolution. Cross sections from the 4-km MM5 forecast along section A–B (see Fig. 7b) were examined to determine the magnitude of the midlevel frontogenesis maximum at the base of the band updraft, the difference of θ_{es} between 600 and 400 hPa on the equatorward flank of the band updraft (a measure of the conditional stability), and the magnitude of the ascent maximum. These parameters were recorded every 15 min during the 1800/25 to 0000/26 time period.

During the time of band formation, the frontogenetical forcing was increasing, while the 600–400-hPa-layer conditional stability was also increasing (Fig. 16). In fact, the smallest θ_{es} difference between 600 and 400 hPa was during the first hour of the time series, when there were shallow, embedded layers of CI (e.g., Fig. 9d). Ascent exceeding 1 m s^{-1} was present from 1830 to 1915/25. This ascent dramatically weakened to 68 cm s^{-1} over the next 45 min as the band formed. Thus, the evolution of ascent, frontogenesis, and conditional stability is consistent with the release of elevated CI in the presence of increasing frontogenetical forcing. The band formed as this instability was released in the sharp convergence zone associated with the developing midlevel trough.

Despite the increasing conditional stability during the time of band maturity, the ascent remained nearly constant near 60 cm s^{-1}. The effect of increasing conditional stability was mitigated by increasing frontogenetical forcing, which reached a peak of 35°C (100 km)$^{-1}$ h^{-1} at 2100/25. After 2100/25, the combined effect of weakening frontogenetical forcing and large conditional stability resulted in band dissipation, with ascent weakening to less than 40 cm s^{-1} by 0000/26. Thus, changes in both the forcing and stability contributed to band dissipation.

5. Moisture availability

In addition to frontogenetical forcing and weak moist symmetric stability, there must be sufficient moisture for band formation to occur. The 12-km MM5 forecast fields were used to determine what role changes in moisture availability in the banded region played in band evolution. However, first the MM5 forecast moisture evolution is validated.

Comparison of observed and forecast IPW values during the 1500/25 to 0300/26 period shows that the MM5 underpredicted IPW on the order of 0.5–1.0 g kg^{-1} (~5%) at all stations except Westford, Massachusetts (Fig. 17). The 0000/26 Albany, New York (ALB), sounding, which was launched in the immediate vicinity of the band, also exhibited a 0.8 g kg^{-1} (~6%) underprediction of IPW (Fig. 17). This small moisture error in the model forecast was likely a contributing factor to the underprediction in precipitation (i.e., Fig. 6). Although there was slightly less moisture modeled in the banded region than observed, the temporal evolution of the moisture fields was well forecast.

To investigate changes in moisture availability, the 12-km MM5 forecast was used to calculate trajectories of parcels that were located in the core of the modeled band updraft at the time of band formation (1930/25),

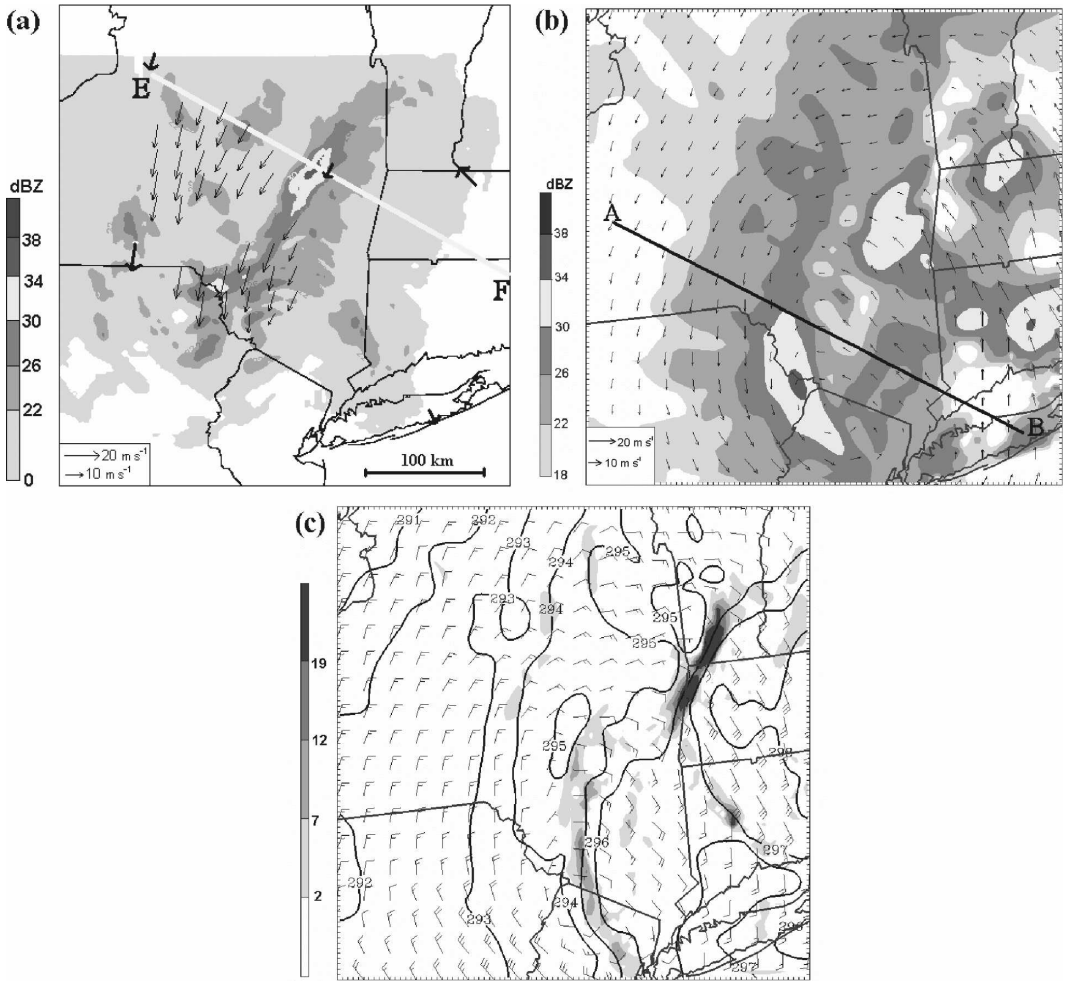

FIG. 14. (a) As in Fig. 7a, except valid at 2359 UTC 25 Dec 2002. (b), (c) As in Figs. 7b,c, but for the 4-km MM5 23-h forecast valid at 2300 UTC 25 Dec 2002.

band maturity (2100/25), and the start of band dissipation (2200/25). The core of the band updraft was located at 500 hPa at 1930 UTC and lowered to 600 hPa at 2100/25 and 2200/25. A total set of 21 trajectories were calculated in seven clusters separated ~50 km apart along the band axis, with each cluster composed of three points aligned across the band axis (separated 12 km apart). Three representative trajectories were chosen at each time to represent parcels on the western side of the band updraft (parcel W), on the eastern side of the band updraft (parcel E), and in the center of the band updraft (parcel C). The location, pressure, temperature, and mixing ratios of all trajectory parcels were recorded every 15 min from the model forecast during the 15-h period from 1200/25 to 0300/26. Mixing ratios are noted at the initial time, the final time, and at the time when the parcels reach 600 hPa in the band updraft. Since the saturation mixing ratio is temperature and pressure dependent, a common pressure level (600 hPa) was chosen to allow comparisons of moisture within the band updraft during band life cycle.

This analysis shows that parcels within the band updraft at 1930/25 originated in the marine boundary layer over the Atlantic Ocean at 1200/25 (Fig. 18a), with initial mixing ratios ranging from 6.7 to 7.7 g kg^{-1} (Fig. 18b). These parcels moved west-northwest and turned cyclonically as they first rose near the surface occluded front, and then rose within the band updraft (Figs. 18a,b). Although a large portion of the original moisture content had precipitated out by the time the parcels arrived at 600 hPa, the parcels retained mixing ratio values between 2.4 and 2.9 g kg^{-1}. The easternmost parcel continued moving to the north-northwest, while parcels farther west turned cyclonically, dramatically illustrating the deformation of the flow. The cyclonically turning trajectories may be considered rep-

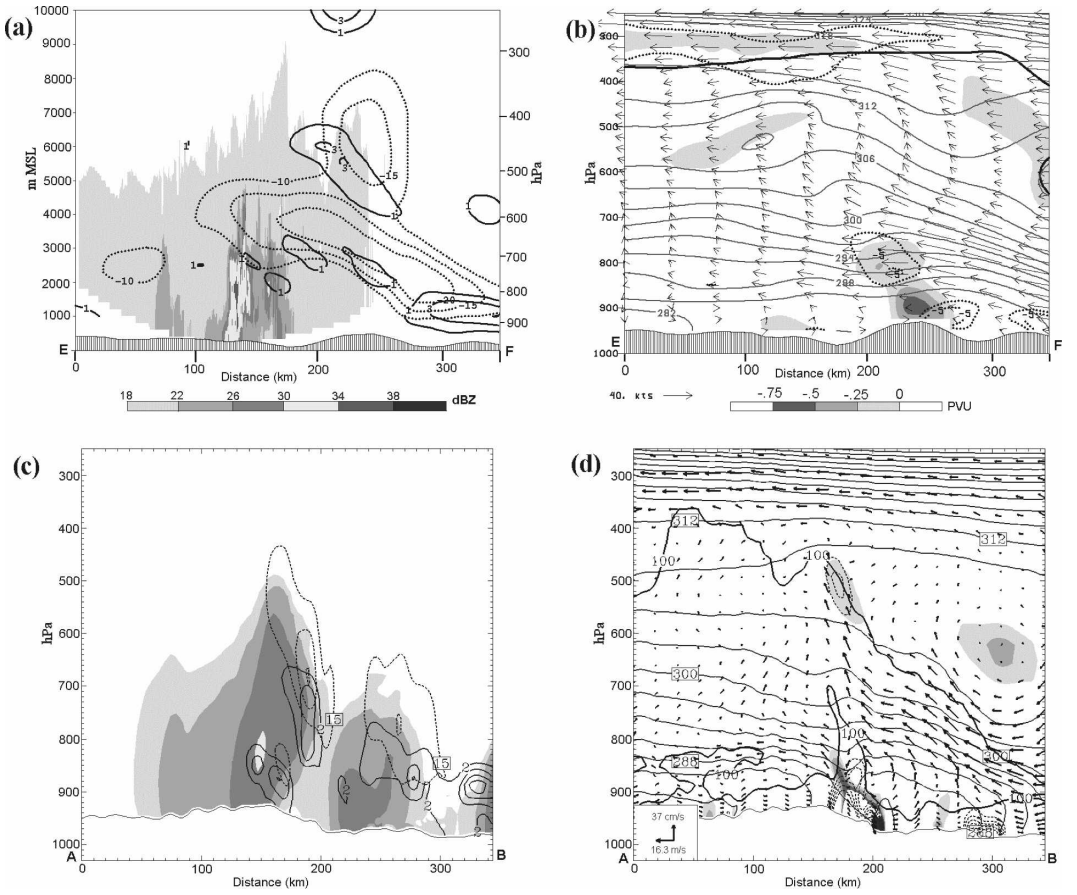

FIG. 15. (a), (b) As in Figs. 12a,b, but for the KENX WSR-88D radar reflectivity cross section (orientation shown in Fig. 15a) valid at 2359 UTC 25 Dec 2002, and Eta analysis fields valid at 0000 UTC 26 Dec 2002. (c), (d) As in Figs. 12c,d, but for the 4-km MM5 23-h forecast valid at 2300 UTC 25 Dec 2002.

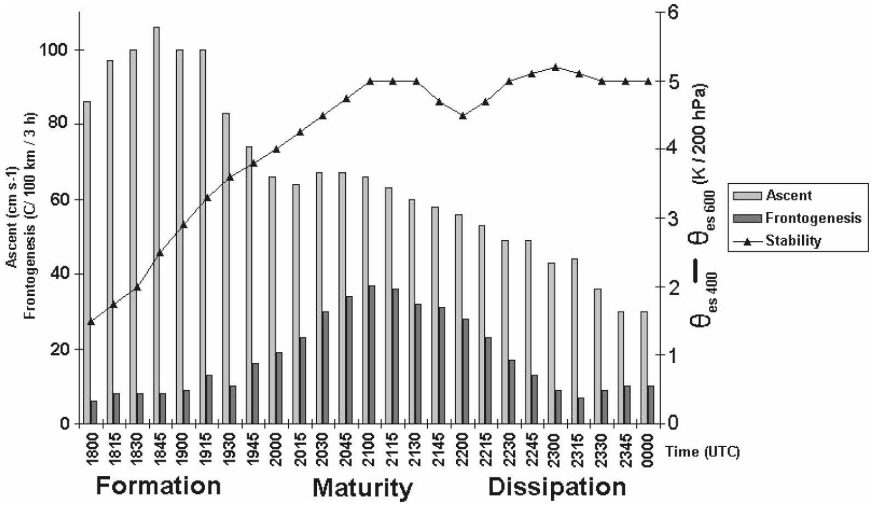

FIG. 16. Time series of midlevel ascent maximum, 2D Miller frontogenesis maximum, and conditional stability in the immediate vicinity of the simulated band. See text for details.

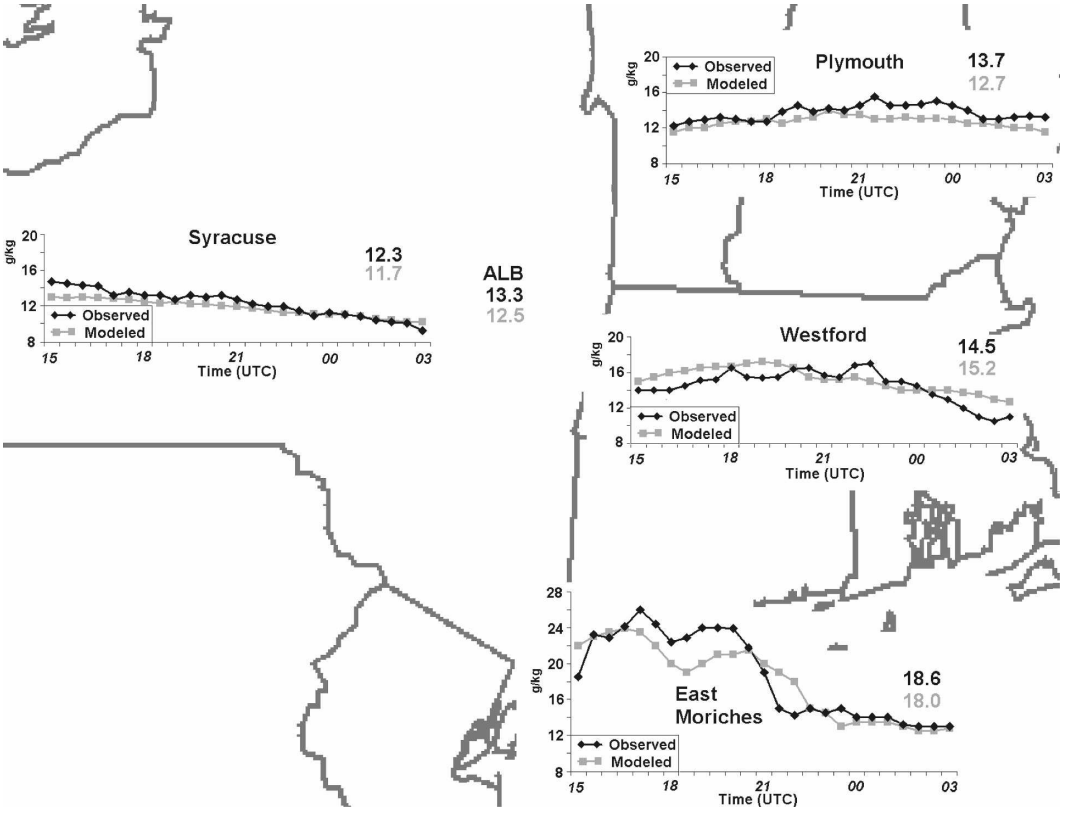

FIG. 17. Time series comparison of 12-km MM5 forecast vs observed integrated precipitable water vapor (g kg^{-1}) from 1500 UTC 25 Dec to 0300 UTC 26 Dec 2002 for Syracuse, NY; Plymouth, NH; Westford, MA; and East Moriches, NY. Mean observed (black) and forecast (gray) values during the time series are shown in upper-right corner of each graph; 0000 UTC 26 Dec 2002 values from the Albany, NY (ALB), operational radiosonde release are also shown.

resentative of the trowal airstream (Martin 1998a,b; Grim et al. 2007; Han et al. 2007), or alternatively the cyclonically turning portion of the warm conveyor belt (Carlson 1980; Schultz 2001).

Parcel trajectories at the start of band dissipation (2200/25) show that the band updraft was composed of two separate airstreams—one originating at low levels over the Atlantic Ocean represented by parcel E, and a second originating well to the south of the banding region, represented by parcels C and W (Figs. 18c,d). As at the time of band formation, parcel E exhibited ascent near the occluded front and within the band updraft; however, the parcel failed to reach 500 hPa in the band updraft (Fig. 18d), indicative of the weaker ascent. Parcels C and W ascended near the surface cyclone, and then experienced more modest ascent in the band updraft after 2100/25, also failing to reach 500 hPa (Figs. 18c,d). Parcel E turned anticyclonically to the north-northeast, while parcels C and W turned cyclonically, illustrating deformation of the flow even at the time of band dissipation. Parcel mixing ratios at 600 hPa within the band updraft at 2200/25 ranged from 2.0 to 2.4 g kg^{-1} (Fig. 18d), which was ~0.4 g kg^{-1} (0.2 g kg^{-1}) less than at the time of band formation (maturity).

The precipitation rate within the modeled band decreased ~30% between 2100/25 and 2200/25 (not shown). To determine what extent changes in moisture and ascent can explain this decrease, parameters from the full set of 21 trajectories were averaged over a 2-h window centered on 2100/25 and 2200/25. A 0.14 g kg^{-1} decrease in water vapor at 600 hPa was recorded between the time of band maturity and band dissipation (Table 1), similar to previously noted changes in parcel C (Fig. 18). Trajectories within the modeled dry slot (e.g., Figs. 2d,f) remained ~50 km to the east of the band updraft, or arrived after band dissipation (not shown). Thus, the dry airstream was not responsible for the decrease in water vapor. Rather, this decrease was due to changes in the thermal profile, as the mean 2100/25 trajectory set conserved a θ_e of 307.2 K during moist ascent during band dissipation, as compared with 308.3 K during band maturity (Table 1). Using the mean

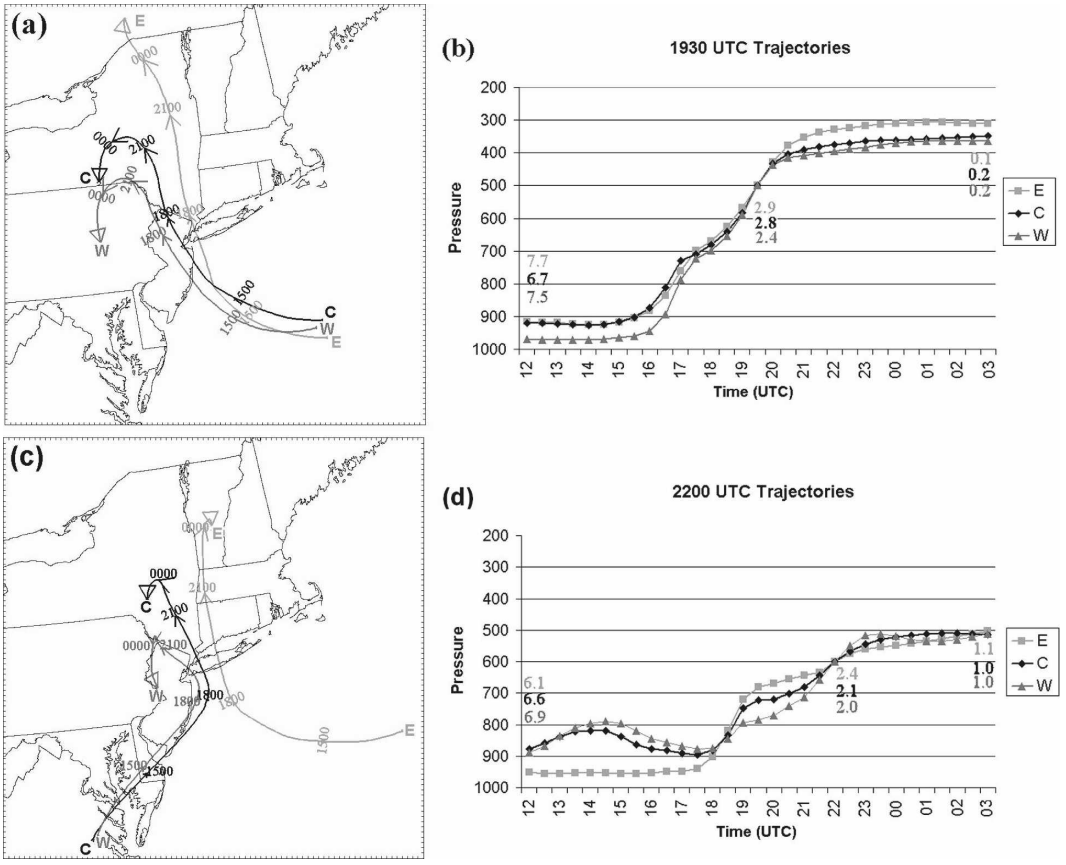

FIG. 18. (a) The 12-km MM5 forecast parcel trajectories passing through the band updraft at 1930 UTC. Time (UTC) labeled on each trajectory path. (b) Time series of parcel trajectory pressure plotted every 0.5 h. Parcel mixing ratios (g kg^{-1}) labeled at the initial time, the final time, and at the time when the parcels reach 600 hPa in the band updraft. (c), (d) As in (a), (b), but for parcel trajectories passing through the band updraft at 2200 UTC 25 Dec 2002.

band maturity θ_e profile, and assuming that all moisture condensed and precipitated, the mean ascent profile during band maturity supported a precipitation rate of 9.8 mm h^{-1}. Using the same ascent profile, but with the cooler θ_e during band dissipation supported a precipitation rate of 9.2 mm h^{-1}, which is 6% less than at the time of band maturity.

The mean ascent averaged among the 21 trajectories decreased markedly between 2100/25 and 2200/25 (Table 1). Using the band maturity moisture profile, assuming all moisture was condensed and precipitated, and substituting the band dissipation ascent profile resulted in a calculated precipitation rate of 7.5 mm h^{-1}, which is 23.5% less than at the time of band maturity. Thus, changes in ascent (indicative of changes in frontogenesis and stability) dominated changes in moisture in explaining band dissipation in this case.

TABLE 1. Comparison of mean trajectory parameters for the time of band maturity (2100 UTC) and the start of band dissipation (2200 UTC).

	Ascent (hPa h^{-1})	600-hPa mixing ratio (g kg^{-1})	Equivalent potential temperature (K)
2100 UTC	73.5	2.25	308.3
2200 UTC	62.5	2.11	307.2

6. Summary and discussion

Dual-Doppler, wind profiler, and aircraft observations in concert with MM5 simulations at 4-km grid spacing were used to investigate the life cycle of an intense mesoscale snowband that occurred 25–26 December 2002. Results from this study show that both the observed and modeled band evolution was related to changes in forcing, stability, and moisture, validating the importance of these parameters in governing band life cycle.

The observations and MM5 forecast show band formation was coincident with the sharpening of a midlevel trough and associated increase in deformation, convergence, and frontogenesis. Although a midlevel trough is evident in previously documented cases (Sanders 1986, his Fig. 6; NG99, their Figs. 4, 9, and 14; Martin 1998a, his Fig. 3), the dual-Doppler observations in the present case help illustrate the pronounced sharpness of the trough and associated wind shift at the time of band formation. Band dissipation occurred as the midlevel trough became less defined and the frontogenetical flow weakened. The weakening frontogenetical forcing in the presence of conditional stability led to a weakening frontal circulation. Future work will investigate the dynamics responsible for the formation and evolution of the midlevel trough in this case, since it is a critical feature of the band life cycle.

Our conventional understanding of the process of band formation relates the reduction of conditional and symmetric stability to band formation. However, the current case exhibited CI at least 1.5 h before band formation (e.g., Fig. 9b). Band formation occurred as this CI was released by increasing frontogenetical forcing, and the conditional stability increased. This result may seem in contrast to the case studies of NG99, in which band formation occurred as the EPV decreased sharply. However, an important difference between the present work and NG99 is that NG99 calculated EPV using the geostrophic wind, which would be more susceptible to the absolute vorticity becoming negative (II). Even in the present case where the full wind is used in calculating EPV, small regions of negative EPV were diagnosed throughout the band life cycle as a symptom of the diabatically generated flow from the band itself. However, just considering the θ_{es} fields in Figs. 5, 10, and 15 of NG99, the smallest conditional stability was observed before band formation, and the conditional stability increased during the band life cycles in each case, as observed and simulated in the present case. A similar stability evolution has been noted by Greenstein (2006, 88–89) in the 6–7 February 2003 and 6 March 2003 northeastern U.S. snowstorms. Additional cases are necessary to determine whether single-band formation may be associated with the transition from a state of elevated CI, to weak conditional and/or moist symmetric stability.

Cross sections through the observed and simulated band revealed that the band core sloped downward to the west at times, which was shown to be a signature of hydrometeor advection. Cross sections also revealed that the ascent maximum was found nearly coincident with the frontogenesis maximum, counter to previous theoretical work, which predicts the ascent maximum 50–200 km on the warm side of the frontal forcing. However, Hakim and Keyser (2001) showed that the value of this displacement is proportional to the static stability and baroclinicity, and inversely proportional to the inertial stability. In the present case, although II was diagnosed in the 400–500-hPa layer, large inertial stability associated with the sharp cyclonic wind shift was diagnosed at the level of maximum frontogenetical forcing (3 km MSL). In this environment the ascent maximum is expected to be closer to the frontogenetical forcing. A component of the displacement discrepancy in this case may also arise from theoretical studies using frontogenetical forcing maximized near the surface (Thorpe and Emanuel 1985; Xu 1992), without a slope (Emanuel 1985), or at a point (Hakim and Keyser 2001), whereas this case exhibits a deep sloping layer of frontogenesis.

Trajectories from the model simulation show that the primary source of moisture during band formation was from the Atlantic Ocean boundary layer. As the band evolved, this moisture-laden airstream was relegated to just the eastern portion of the band, while the remaining length of the band was being fed by slightly colder (drier) air originating in the midlevels to south of the banding region. This change in moisture was calculated to result in a 6% reduction in precipitation rate. A larger reduction in precipitation rate (23%) was calculated due to changing ascent. Thus the effect of changing ascent (indicative of changes in frontogenesis and stability) dominated over changing moisture in explaining band dissipation in this case.

Maximum precipitation was underforecast within the banded region by ~30% at 4-km grid spacing, and the axis of heaviest precipitation was displaced ~50 km to the southeast of the observed location. Comparisons between high-resolution observations and the model forecasts show that the band position error was tied to an error in the location of the midlevel trough and subsequent location of mesoscale forcing. The early weakening of this trough and associated frontogenesis in the presence of stronger conditional stability than analyzed led to premature band dissipation in the MM5 forecast. The greater stability and shorter band duration in the MM5 forecast likely accounted for a majority of the precipitation underprediction, although a small underprediction of integrated precipitatable water vapor in the banded region also likely contributed. Higher horizontal model resolution was shown to contribute toward improved QPF; however, it appears more dramatic improvement may be gained by better simulating the frontogenesis, stability, and moisture evolution in this case.

This study illustrates that mesoscale models are ca-

pable of generating realistic snowbands; however, the intrinsic uncertainties associated with forecasting the evolution of forcing, stability, and moisture suggest improved forecasts of mesoscale bands and the resulting QPF will likely require ensemble approaches. Additional observations of temperature, vertical velocities, and microphysics may also further our understanding of the structural and dynamical evolution of banded events and help diagnose model deficiencies. Future work will draw on high-resolution observations and model forecasts of additional banded snowfall events to further generalize the study results and explore ensemble approaches to band prediction.

Acknowledgments. The authors thank Greg Hakim (U-Washington), Daniel Keyser (SUNY Albany), Mark Stoelinga (U-Washington), David Schultz (U-Helsinki/FMI), Jeff Waldstreicher (NOAA/NWS), and three anonymous reviewers for insightful comments concerning this work. Catherine Spooner (NCSU) performed the WSR-88D dual-Doppler synthesis. This study was supported in part by the National Science Foundation under Grants ATM 0450444 (Colle), and 0121963 and 0544766 (Yuter).

REFERENCES

Baxter, M. A., and C. E. Graves, 2006: A case example of the role of warm-sector convection in the development of mesoscale banded snowfall: 2003 November 22–24. Preprints, *23rd Conf. on Severe Local Storms,* St. Louis, MO, Amer. Meteor. Soc., 4.6.

Benjamin, S. G., G. A. Grell, J. M. Brown, T. G. Smirnova, and R. Bleck, 2004: Mesoscale weather prediction with the RUC hybrid isentropic–terrain-following coordinate model. *Mon. Wea. Rev.,* **132,** 473–494.

Bennetts, D. A., and B. J. Hoskins, 1979: Conditional symmetric instability—A possible explanation for frontal rainbands. *Quart. J. Roy. Meteor. Soc.,* **105,** 945–962.

Browning, K. A., 1990: Organization of clouds and precipitation in extratropical cyclones. *Extratropical Cyclones: The Erik Palmén Memorial Volume,* C. W. Newton and E. O. Holopainen, Eds., Amer. Meteor. Soc., 129–153.

Cao, Z., and H.-R. Cho, 1995: Generation of moist potential vorticity in extratropical cyclones. *J. Atmos. Sci.,* **52,** 3263–3282.

Carlson, T. N., 1980: Airflow through midlatitude cyclones and the comma cloud pattern. *Mon. Wea. Rev.,* **108,** 1498–1509.

Clark, J. H. E., R. P. James, and R. H. Grumm, 2002: A reexamination of the mechanisms responsible for banded precipitation. *Mon. Wea. Rev.,* **130,** 3074–3086.

Dudhia, J., 1989: Numerical study of convection observed during the winter monsoon experiment using a mesoscale two-dimensional model. *J. Atmos. Sci.,* **46,** 3077–3107.

——, 1993: A nonhydrostatic version of the Penn State–NCAR mesoscale model: Validation tests and simulation of an Atlantic cyclone and cold front. *Mon. Wea. Rev.,* **121,** 1493–1513.

Eliassen, A., 1962: On the vertical circulation in frontal zones. *Geophys. Publ.,* **24,** 147–160.

Emanuel, K. A., 1985: Frontal circulations in the presence of small moist symmetric stability. *J. Atmos. Sci.,* **42,** 1062–1071.

Greenstein, M. D., 2006: Mesoscale structure of precipitation regions in northeast winter storms. M.S. thesis, Dept. of Earth and Atmospheric Sciences, University at Albany, State University of New York, 116 pp.

Grell, G. A., 1993: Prognostic evaluation of assumptions used by cumulus parameterizations. *Mon. Wea. Rev.,* **121,** 764–787.

Grim, J. A., R. M. Rauber, M. K. Ramamurthy, B. F. Jewett, and M. Han, 2007: High-resolution observations of the trowal–warm-frontal region of two continental winter cyclones. *Mon. Wea. Rev.,* **135,** 1629–1646.

Gutman, S. I., S. R. Sahm, S. G. Benjamin, B. E. Schwartz, K. L. Holub, J. Q. Stewart, and T. L. Smith, 2004: Rapid retrieval and assimilation of ground based GPS precipitable water observations at the NOAA Forecast Systems Laboratory: Impact on weather forecasts. *J. Meteor. Soc. Japan,* **82,** 351–360.

Hakim, G. J., and D. Keyser, 2001: Canonical frontal circulation patterns in terms of Green's functions for the Sawyer–Eliassen equation. *Quart. J. Roy. Meteor. Soc.,* **127,** 1795–1814.

Han, M., R. M. Rauber, M. K. Ramamurthy, B. F. Jewett, and J. A. Grim, 2007: Mesoscale dynamics of the trowal and warm-frontal regions of two continental winter cyclones. *Mon. Wea. Rev.,* **135,** 1647–1670.

Hobbs, P. V., J. D. Locatelli, and J. E. Martin, 1996: A new conceptual model for cyclones generated in the lee of the Rocky Mountains. *Bull. Amer. Meteor. Soc.,* **77,** 1169–1178.

Holt, M. W., and A. J. Thorpe, 1991: Localized forcing of slantwise motion at fronts. *Quart. J. Roy. Meteor. Soc.,* **117,** 943–963.

Hong, S.-Y., and H.-L. Pan, 1996: Nonlocal boundary layer vertical diffusion in a medium-range forecast model. *Mon. Wea. Rev.,* **124,** 2322–2339.

——, J. Dudhia, and S.-H. Chen, 2004: A revised approach to ice microphysical processes for the bulk parameterization of clouds and precipitation. *Mon. Wea. Rev.,* **132,** 103–120.

Houze, R. A., Jr., P. V. Hobbs, K. R. Biswas, and W. M. Davis, 1976: Mesoscale rainbands in extratropical cyclones. *Mon. Wea. Rev.,* **104,** 868–879.

Jurewicz, M. L., Sr., and M. S. Evans, 2004: A comparison of two banded, heavy snowstorms with very different synoptic settings. *Wea. Forecasting,* **19,** 1011–1028.

Keyser, D., B. D. Schmidt, and D. G. Duffy, 1992: Quasigeostrophic vertical motions diagnosed from along- and cross-isentrope components of the **Q** vector. *Mon. Wea. Rev.,* **120,** 731–741.

Klazura, G. E., and D. A. Imy, 1993: A description of the initial set of analysis products available from the NEXRAD WSR-88D system. *Bull. Amer. Meteor. Soc.,* **74,** 1293–1311.

Koch, S. E., B. Ferrier, M. T. Stoelinga, E. Szoke, S. J. Weiss, and J. S. Kain, 2005: The use of simulated radar reflectivity fields in the diagnosis of mesoscale phenomena from high-resolution WRF model forecasts. Preprints, *32nd Conf. on Radar Meteorology,* Albuquerque, NM, Amer. Meteor. Soc., J4J.7.

Kocin, P. J., and L. W. Uccellini, 2004: *Northeast Snowstorms*. Vol. 1. *Meteor. Monogr.,* No. 54, Amer. Meteor. Soc., 296 pp.

Leise, J. A., 1982: A multidimensional scale-telescoped filter and data extension package. NOAA Tech. Memo. ERL WPL-82, 19 pp.

Martin, J. E., 1998a: The structure and evolution of a continental winter cyclone. Part I: Frontal structure and the occlusion process. *Mon. Wea. Rev.,* **126,** 303–328.

——, 1998b: The structure and evolution of a continental winter cyclone. Part II: Frontal forcing of an extreme snow event. *Mon. Wea. Rev.,* **126,** 329–348.

——, 1999: Quasigeostrophic forcing of ascent in the occluded sector of cyclones and the trowal airstream. *Mon. Wea. Rev.,* **127,** 70–88.

Michalakes, J., S. Chen, J. Dudhia, L. Hart, J. Klemp, J. Middlecoff, and W. Skamarock, 2001: Development of a next generation regional weather research and forecast model. *Developments in Teracomputing: Proc. Ninth ECMWF Workshop on the Use of High Performance Computing in Meteorology,* Reading, United Kingdom, European Centre for Medium-Range Weather Forecasts, 269–276.

Miller, J. E., 1946: Cyclogenesis in the Atlantic coastal region of the United States. *J. Meteor.,* **3,** 31–44.

——, 1948: On the concept of frontogenesis. *J. Meteor.,* **5,** 169–171.

Mohr, C. G., L. J. Miller, R. L. Vaughn, and H. W. Frank, 1986: The merger of mesoscale datasets into a common Cartesian format for efficient and systematic analyses. *J. Atmos. Oceanic Technol.,* **3,** 143–161.

Moninger, W. R., R. D. Mamrosh, and P. M. Pauley, 2003: Automated meteorological reports from commercial aircraft. *Bull. Amer. Meteor. Soc.,* **84,** 203–216.

Moore, J. T., C. E. Graves, S. Ng, and J. L. Smith, 2005: A process-oriented methodology toward understanding the organization of an extensive mesoscale snowband: A diagnostic case study of 4–5 December 1999. *Wea. Forecasting,* **20,** 35–50.

Morcrette, C. J., and K. A. Browning, 2006: Formation and release of symmetric instability following Delta-M adjustment. *Quart. J. Roy. Meteor. Soc.,* **132,** 1073–1089.

Nicosia, D. J., and R. H. Grumm, 1999: Mesoscale band formation in three major northeastern United States snowstorms. *Wea. Forecasting,* **14,** 346–368.

Novak, D. R., and B. A. Colle, 2005: Comparison of MM5 and WRF forecasts of the 25 December 2002 northeast U.S. banded snowstorm. Preprints, *Sixth WRF/15th MM5 User's Workshop,* Boulder, CO, National Center for Atmospheric Research, 1.4.

——, L. F. Bosart, D. Keyser, and J. S. Waldstreicher, 2004: An observational study of cold season–banded precipitation in northeast U.S. cyclones. *Wea. Forecasting,* **19,** 993–1010.

——, J. S. Waldstreicher, D. Keyser, and L. F. Bosart, 2006: A forecast strategy for anticipating cold season mesoscale band formation within eastern U.S. cyclones. *Wea. Forecasting,* **21,** 3–23.

Persson, P. O. G., and T. T. Warner, 1993: Nonlinear hydrostatic conditional symmetric instability: Implications for numerical weather prediction. *Mon. Wea. Rev.,* **121,** 1821–1833.

——, and ——, 1995: The nonlinear evolution of idealized, unforced, conditional symmetric instability: A numerical study. *J. Atmos. Sci.,* **52,** 3449–3474.

Ralph, F. M., and Coauthors, 2005: Improving short-term (0–48 h) cool-season quantitative precipitation forecasting: Recommendations from a USWRP workshop. *Bull. Amer. Meteor. Soc.,* **86,** 1619–1632.

Reuter, G. W., and M. K. Yau, 1990: Observations of slantwise convective instability in winter cyclones. *Mon. Wea. Rev.,* **118,** 447–458.

Rogers, E., T. Black, B. Ferrier, Y. Lin, D. Parrish, and G. DiMego, 2001: Changes to the NCEP Meso Eta Analysis and Forecast System: Increase in resolution, new cloud microphysics, modified precipitation assimilation, modified 3DVAR analysis. NOAA/NWS Tech. Procedures Bulletin 488, National Weather Service, 21 pp. [Available online at http://www.emc.ncep.noaa.gov/mmb/mmbpll/eta12tpb.]

Sanders, F., 1986: Frontogenesis and symmetric stability in a major New England snowstorm. *Mon. Wea. Rev.,* **114,** 1847–1862.

——, and L. F. Bosart, 1985: Mesoscale structure in the megalopolitan snowstorm of 11–12 February 1983. Part I: Frontogenetical forcing and symmetric instability. *J. Atmos. Sci.,* **42,** 1050–1061.

Sawyer, J. S., 1956: The vertical circulation at meteorological fronts and its relation to frontogenesis. *Proc. Roy. Soc. London,* **A234,** 346–362.

Schultz, D. M., 2001: Reexamining the cold conveyor belt. *Mon. Wea. Rev.,* **129,** 2205–2225.

——, and P. N. Schumacher, 1999: The use and misuse of conditional symmetric instability. *Mon. Wea. Rev.,* **127,** 2709–2732; Corrigendum, **128,** 1573.

——, and J. A. Knox, 2007: Banded convection caused by frontogenesis in a conditionally, symmetrically, and inertially unstable environment. *Mon. Wea. Rev.,* **135,** 2095–2110.

Stensrud, D. J., and Coauthors, 2006: The New England high-resolution temperature program. *Bull. Amer. Meteor. Soc.,* **87,** 491–498.

Stewart, R. E., 1991: Canadian Atlantic Storms Program: Progress and plans of the meteorological component. *Bull. Amer. Meteor. Soc.,* **72,** 364–371.

Stuart, N. A., and R. H. Grumm, 2006: Using wind anomalies to forecast East Coast winter storms. *Wea. Forecasting,* **21,** 952–968.

Thorpe, A. J., and K. A. Emanuel, 1985: Frontogenesis in the presence of small stability to slantwise convection. *J. Atmos. Sci.,* **42,** 1809–1824.

——, and S. A. Clough, 1991: Mesoscale dynamics of cold fronts: Structures described by dropsoundings in FRONTS 87. *Quart. J. Roy. Meteor. Soc.,* **117,** 903–941.

Wiesmueller, J. L., and S. M. Zubrick, 1998: Evaluation and application of conditional symmetric instability, equivalent potential vorticity, and frontogenetic forcing in an operational forecasting environment. *Wea. Forecasting,* **13,** 84–101.

Xu, Q., 1989: Extended Sawyer–Eliassen equation for frontal circulations in the presence of small viscous moist symmetric stability. *J. Atmos. Sci.,* **46,** 2671–2683.

——, 1992: Formation and evolution of frontal rainbands and geostrophic potential vorticity anomalies. *J. Atmos. Sci.,* **49,** 629–648.

Yuter, S. E., and R. A. Houze Jr., 1995: Three-dimensional kinematic and microphysical evolution of Florida cumulonimbus. Part I: Spatial distribution of updrafts, downdrafts, and precipitation. *Mon. Wea. Rev.,* **123,** 1921–1940.